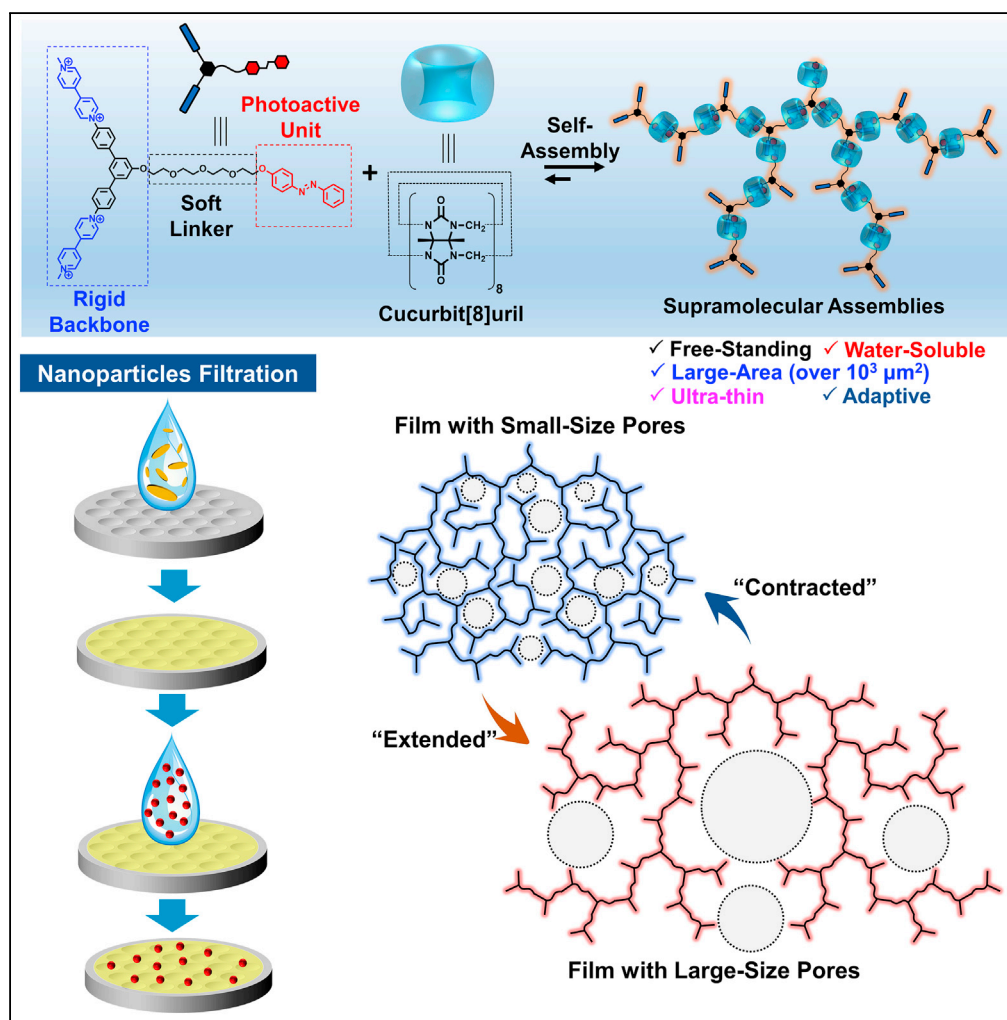**Article**

Dynamic Adaptive Two-Dimensional Supramolecular Assemblies for On-Demand Filtration

Qi Zhang, Ruo-Jie Xing, Wen-Zhi Wang, Yuan-Xin Deng, Da-Hui Qu, He Tian

dahui_qu@ecust.edu.cn

HIGHLIGHTS

2D supramolecular assemblies combine large area, nano-thickness and water solubility

The 2D assemblies can perform reversible expansion/contraction to tune pore sizes

The 2D material can be used for on-demand nanoparticles filtration

Article

Dynamic Adaptive Two-Dimensional Supramolecular Assemblies for On-Demand Filtration

Qi Zhang,[1,2] Ruo-Jie Xing,[1,2] Wen-Zhi Wang,[1] Yuan-Xin Deng,[1] Da-Hui Qu,[1,3,*] and He Tian[1]

SUMMARY

The construction of synthetic two-dimensional (2D) materials designates a pathway to the versatile chemical functionality by spatial control. However, current 2D materials with intelligence of stimuli-responsibility and adaptiveness have been unfledged. The approach reported here uses a supramolecular strategy to achieve the dynamic non-covalent self-assembly of a rationally designed small molecule monomer, producing large-area, ultra-thin, porous 2D supramolecular assemblies, which are solution-processable in aqueous solution. Importantly, the 2D supramolecular assemblies exhibit distinct adaptive capability to automatically regulate their network density and pore diameters in response to environmental temperature change, which could be developed into an "on-demand" filtration application for nanoparticles. Meanwhile, the 2D supramolecular assemblies can also perform reversible degradation/reformation by photo-irradiation. Our results not only show the simplicity, reliability, and effectiveness of supramolecular strategies in the construction of 2D materials with practical sizes, but also push the dynamic alterability and adaptation features from supramolecular assemblies toward 2D materials.

INTRODUCTION

The design and fabrication of supramolecular polymers and materials by precise "bottom-up" self-assembly of building blocks has been an appealing and vital theme for chemists owing to the distinct dynamic properties of supramolecular materials (Lutz et al., 2016; Yang et al., 2015; Yu et al., 2015; Amabilino et al., 2017; Krieg et al., 2016; Chen and Liu, 2015; Qu et al., 2015; Zhang et al., 2018a, 2018b, 2018c, 2018d). Many efforts have been realized in the constructions of sophisticated supramolecular architectures by elaborating the structural design of building blocks and controlling the dimensions, sizes, and manners of the further self-assembly to form diversified supramolecular materials exhibiting the superiority and functionality (Yu et al., 2018; Sun et al., 2018; Zhang et al., 2018a, 2018b, 2018c, 2018d; Xing et al., 2018; Ji et al., 2018; Tian et al., 2014; Tao et al., 2019). Meanwhile, man-made 2D organic materials have also attracted much attention of chemists since the rise of graphene (Colson and Dichtel, 2013; Zhuang et al., 2015). Although amounts of 2D metal/covalent organic frameworks have been built and fabricated by different kinds of synthetic methodologies and libraries (Wang et al., 2018a, 2018b, 2018c, 2019; Baek et al., 2013; Matsumoto et al., 2018; Xiao et al., 2018), the design and construction of 2D supramolecular assemblies are still under fledging stage, especially those exhibiting large-area, ultra-thin, free-standing, water-soluble features (Zhang et al., 2013; Pfeffermann et al., 2015; Yue et al., 2016).

A reasonable strategy to fabricate 2D supramolecular assemblies involves the design of rigid and multi-branched monomers, which would define the assemblies growth in a highly ordered direction, resulting in rigid supramolecular frameworks (Dong et al., 2018). However, the strictly rigid structure mostly inhibited the large-area polymer growth because of the vertical packing tendency of rigid structures and the lack of flexibility, which is significant to allow the adaptive interactions among small-molecular-weight 2D assemblies with different edge shapes. Some groups strive to overcome this issue by interfacial self-assembly strategy (Pfeffermann et al., 2015; Dong et al., 2018), however, requiring special processing technique. Flexible hyperbranched monomers are good examples to form large-size supramolecular assemblies (Huang and Gibson, 2004; Fernández et al., 2008; Zhou et al., 2010; Dong et al., 2011a, 2011b, 2014; Tao et al., 2012; Fang et al., 2013; Wang et al., 2014) but remain a challenging issue how to precisely construct the dimensions of the assemblies. In many cases, such flexible hyperbranched building blocks tend to self-assemble into spheres or particles because of the flexibility-induced surface curving (Dong et al., 2011a, 2011b; Groombridge et al., 2017; Tian et al., 2017; Datta et al., 2018; Liu
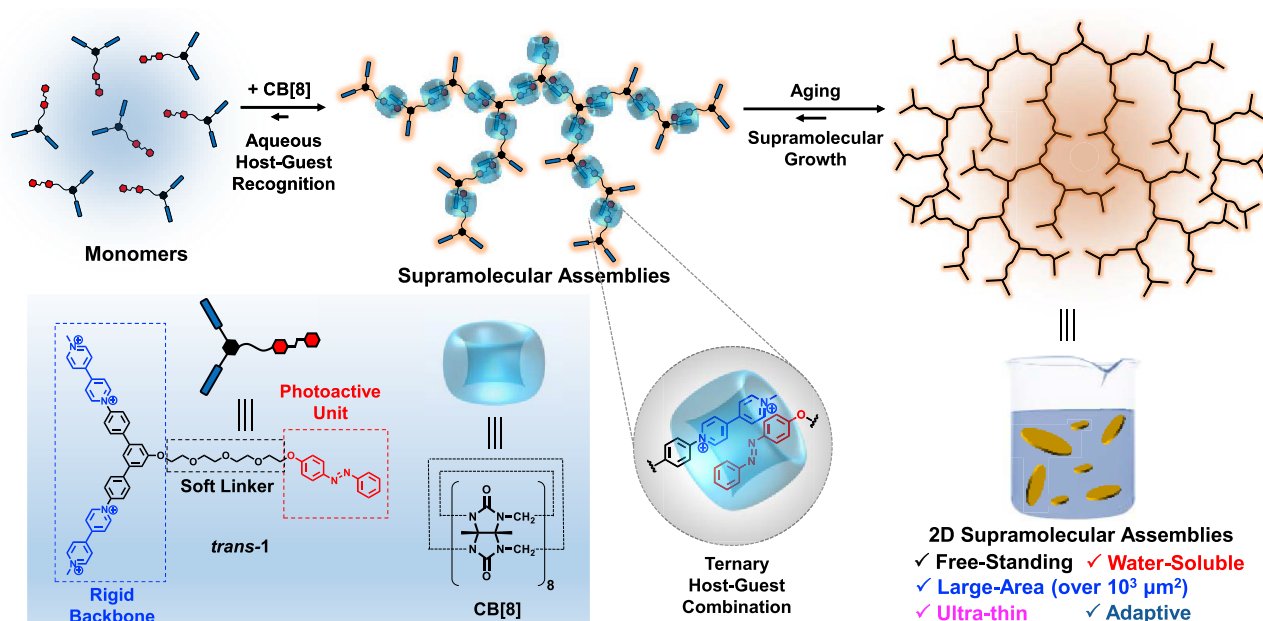
Figure 1. Schematic Illustration and Molecular Structure

The molecular structure of *trans*-1 and the schematic representation of the supramolecular assemblies of *trans*-1 and CB[8]. The backbone of the final assemblies is simplified for clear presentation.

et al., 2018). Hence, it is still a fundamental question of whether the 2D supramolecular assemblies with large area can be achieved by the direct solution-phase growth strategies rather than by the self-assembly on interfaces/surfaces.

Meanwhile, one of the representative features of supramolecular assemblies involves the capability of stimuli-responsive materials owing to the unique dynamic nature. Numerous supramolecular assemblies, such as zero-dimensional vesicle/micelle (Gaitzsch et al., 2016; Wang et al., 2018a, 2018b, 2018c; Gao et al., 2018; Chen et al., 2018; Hu et al., 2018), one-dimensional fibers/tubes (Hendricks et al., 2017; Cohen et al., 2018; Yagai et al., 2019), and three-dimensional gels (Appel et al., 2012; Jones and Steed, 2016; Voorhaar and Hoogenboom, 2016), have been proved to be talented in many potential applications. However, the alterability and stimuli-responsive behavior of 2D supramolecular assemblies have not been exploited yet. Hence, our motivation in these issues locates on following two original hypotheses: (1) whether we can enable the structural rigidity and flexibility in a single 2D supramolecular assembly; (2) what unprecedented properties and functions can be brought in this rigid and flexible 2D supramolecular assemblies. Herein, we report a rationally designed 2D supramolecular assembly to demonstrate the above-mentioned proposals, achieving the direct aqueous self-assembly to form 2D supramolecular assemblies that integrate large area (up to 1000 μm^2), nano-sized thickness, water-solubility, and stimuli-induced alterability.

In our design, a semi-rigid tri-branch compound *trans*-1 was constructed (Figure 1). The unique Y-type structure bears two viologen units and a single azobenzene unit, which can bind together in the cavity of macrocycle cucurbit[8]uril (CB[8]) to form high-affinity ternary host-guest complex (Barrow et al., 2015; Del Barrio et al., 2013; Tian et al., 2012; Pazos et al., 2019). Notably, the viologen-terminated aromatic part bears a rigid backbone with a fixed angle of 120°, whereas the azobenzene-terminated linker is flexible. This semi-rigid design is expected to enable a dendrimer-like supramolecular self-assembly in aqueous solution. We expect that the rigid 120° aromatic backbone could support sufficient space for the tubular macrocycle CB[8] and hence inhibit the steric-hindrance-caused low polymerization degree of the supramolecular assemblies. Meanwhile, the simultaneous presence of soft glycol linker provides flexibility to the resulting supramolecular assemblies. This design is distinct from the previously reported strictly rigid supramolecular frameworks, in which the polymer skeleton is rigid and stable. It is expected that our "semi-rigid" design could generate a unique large-sized supramolecular assembly that simultaneously exhibits the capability of dynamic stimuli responsiveness and adaptiveness.

RESULTS AND DISCUSSION

The compound *trans*-1 was synthesized. Starting with a previously reported compound **2** (Wang et al., 2017), two steps of etherification reactions were performed to yield compound **3** and **4**. Then the trifluoro-acetic acid (TFA) was used to deprotect the phenylamine groups, and triethylamine was used to neutralize the mixture to expose the amino groups. Finally, the target compound *trans*-1 was produced by the Zinke reaction with compound **5**. The detailed synthesis route of compound *trans*-1 has been shown in the experimental section of Supplemental Information. The compound structure has been well characterized and confirmed by NMR and HR-MS (see in Supplemental Information).

Trans-1 exhibits water solubility owing to the presence of two hydrophilic viologen units, thus producing a homogeneous aqueous solution. The host-guest recognition of *trans*-1 with macrocycle CB[8] was confirmed by the observed shielded and broadened aromatic peaks of *trans*-1 after addition of CB[8] in ^{1}H NMR spectra (Figure S1). In the UV-Vis spectra titration experiment (Figure 2A), a remarkable intensity decrease was observed in both the peaks at 260 and 345 nm with the CB[8] solution added, which are attributed to the viologen units and the azobenzene units, respectively. Meanwhile, a shoulder peak after 400 nm rise with the addition of 1.5 equivalents CB[8], and resulted in an isoabsorptive point observed at 400 nm, indicating the formation of the proposed ternary host-guest combination.

Considering the hyperbranched molecular structure of *trans*-1, the CB[8]-mediated host-guest combination should generate supramolecular assembled networks. Dynamic light scattering (DLS) indicated the large-sized assemblies in the aqueous solution of *trans*-1 after mixing with 1.5 equivalents of CB[8] (Figure 2B). Tyndall effect can be also visible after the addition of CB[8], whereas no visible Tyndall effect can be found in the aqueous solution of *tran*-1 (Figure 2B inset). Transmission electron microscopy (TEM) images showed the morphology of the formed supramolecular assemblies, which are micron-sized and have a homogeneous thickness distribution (Figure 2C). Notably, some edge regions of the assemblies were found to be branched (Figure S2), suggesting a highly dynamic nature at the edge region of the supramolecular assemblies. The area of these supramolecular assemblies was found to be as large as over 1,000 μm² measured by optical microscopy image (Figure 2D). The large-area supramolecular assemblies can be processed into a free-standing dry film by simple drop-casting method (Figure S3). The resulting supramolecular assemblies exhibited a reasonable broad scattering peak in small-angle X-ray scattering (SAXS) pattern (Figure S4), indicating the relatively low long-range order in the assembled network, which is consistent with the proposed dendrimer-like supramolecular assembling mode (Figure 1).

The thickness of the supramolecular assemblies was measured as 5.26 ± 0.10 nm by atomic force microscopy (AFM) (Figures 2E and 2F). Considering the 1.75-nm outer diameter of CB[8] macrocycle (Zhang et al., 2013), the film should be of few layers. This observation is also reasonable because of the micron-sized area of this 2D material in aqueous solution, which would lead to a thermodynamics-preferred packing process. The area-to-thickness of the film can be up to 19 cm. To the best of our knowledge, the observed large area (1,320 μm²) and large area-to-thickness ratio have never been achieved previously in 2D supramolecular assemblies formed by direct aqueous self-assembly process. The large-scale and ultrathin supramolecular assemblies should be attributed to the following four factors: (1) the high binding affinity of the CB[8] ternary host-guest combination as the noncovalent interaction in the network; (2) semi-rigid molecular design of the monomer, whose rigidity supports the spatial 2D extension toward large scale, and the flexibility simultaneously allows the solubility by inhibiting rigid-packing-caused crystalline process; (3) the tubular CB[8] macrocycles effectively decrease the interlayer packing, and the intrinsic rigidity also supports the orientated ternary host-guest combinations, which is necessary for large-scale 2D extension; (4) the paralleled 1:1:1 ternary host-guest combination between MV²⁺ and azobenzene units inside the cavity of CB[8] might also facilitate the further planar growth of the 2D assemblies. However, despite the presence of such large-sized assemblies, the aqueous solution of the supramolecular assemblies is homogeneous, transparent, and stable for months. Therefore, this rational design enables a successful solution-phase growth of micro-area, nano-thickness 2D supramolecular assembly via a simple supramolecular self-assembly strategy.

Interestingly, we found that the resulting 2D supramolecular assemblies exhibited temperature-adaptive deformable ability. After heating the aqueous solution of assemblies at 40°C for 1 h, the 2D supramolecular assemblies transformed from 2D assemblies into highly branched networks (Figures 3A–3D and S5). The observed transformation of the 2D assemblies should be explained as the entropy-driven expansion from high-density
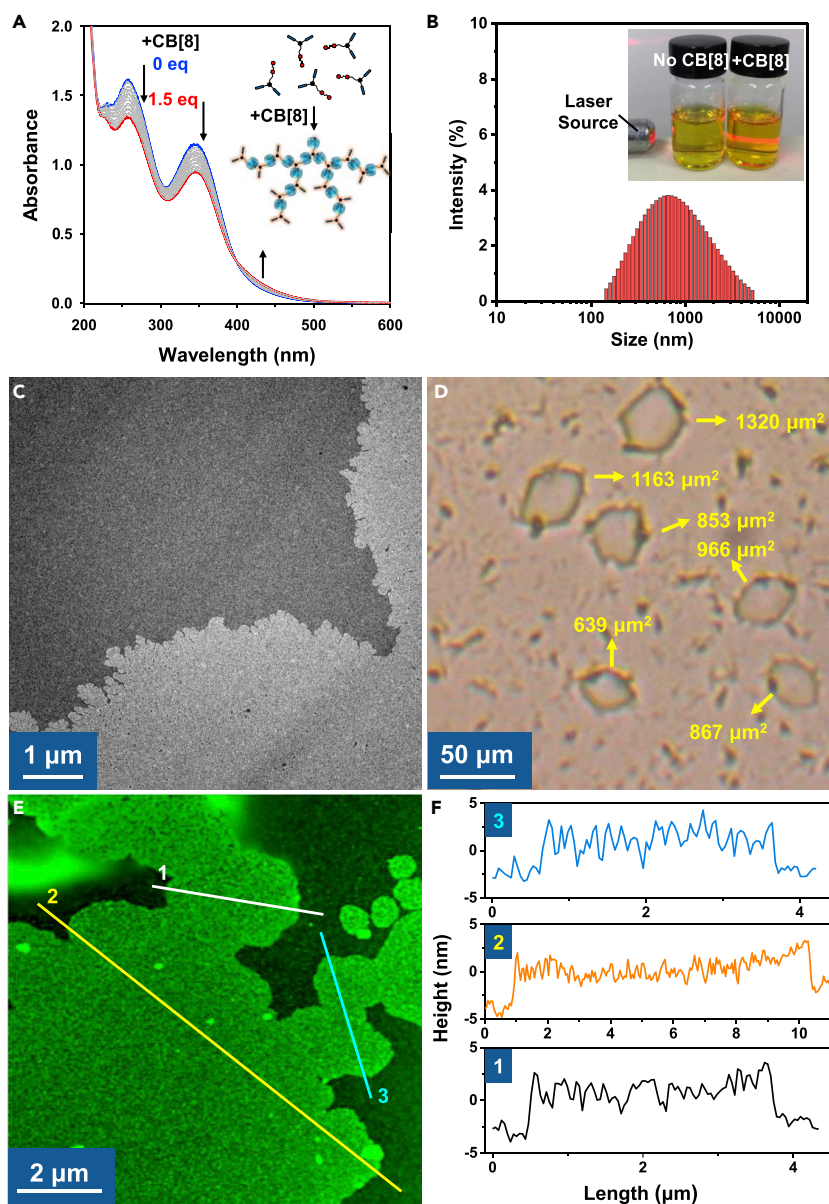
Figure 2. Optical Properties and Morphology of the Supramolecular Assemblies

(A) UV-Vis absorption spectra of the titration experiment of *trans*-**1** (50 μM in H_2O) upon addition of CB[8].

(B) DLS result of the mixed aqueous solution of *trans*-**1** (1 mM in H_2O; 25°C) after addition of 1.5 equivalents CB[8]. The inset image shows the different Tyndall effect of the *trans*-**1** aqueous solutions (1 mM) without (left) and with (right) CB[8].

(C) TEM image of the supramolecular assemblies.

(D) Optical microscopy image of the supramolecular assemblies.

(E) AFM image of the supramolecular assemblies.

(F) Section height analysis of the corresponding linear region in (E).

dendrimer-like network to disordered low-density branched network. Notably, the porous structure on the assemblies at 0°C can be observed in TEM image with higher magnification (Figure 3B inset). The porous structure can be attributed to the intrinsic space in dendrimer-like network of the resulting supramolecular assemblies. The expansion consequently resulted in the diameter increase of the film pores from about 5 nm (0°C) to about 40 nm (40°C) (Figures 3C–3E). The expansion of the pores might be attributed to the heat-accelerated dynamic exchange process between assemblies and free monomers/oligomers, resulting in the increase in the ratio of the "active" edges, which induced the expansion deformation of the supramolecular film into a highly branched
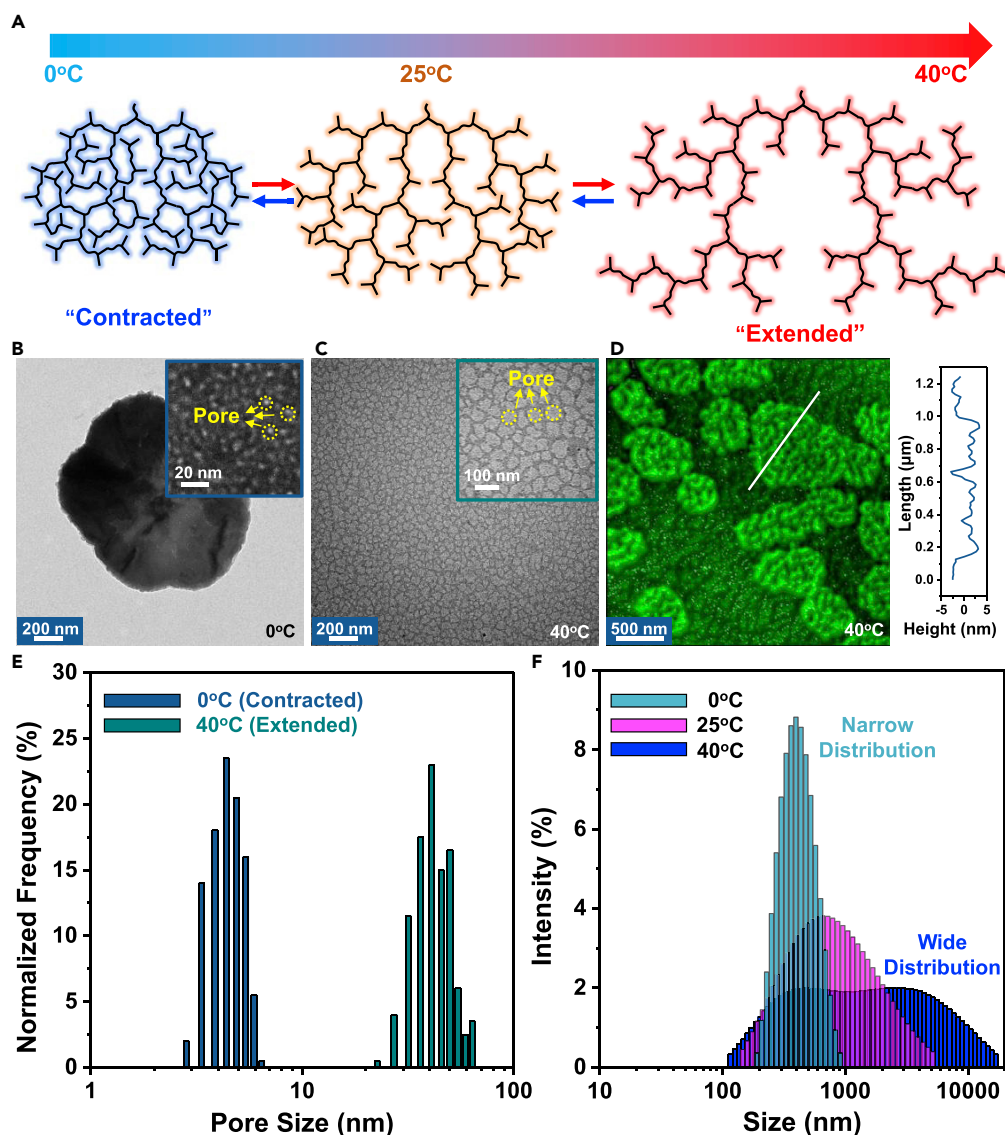
Figure 3. Reversible Contraction/Expansion Behavior by Thermally Adaptive Deformation

(A) Schematic representation of the thermal deformation of the supramolecular assemblies between 2D film and hyper-branched network.

(B) TEM images of the supramolecular assemblies at 0°C. Inset image shows the pores with nanometer diameter.

(C) TEM images of the supramolecular assemblies at 40°C. Inset image shows the "extended" pores with larger diameter.

(D) AFM images and section height analysis of the 2D supramolecular assemblies at 40°C.

(E) Normalized frequency distribution of the pore diameter of the 2D assemblies at 0°C and 40°C. The statistical data were collected from 200 randomly selected pores in TEM images.

(F) DLS results of the supramolecular polymers *trans*-1@CB[8] solution (1 mM, H$_2$O) at varied temperature.

network with more "active" edges. Furthermore, the morphology of the supramolecular assemblies at lower temperature (0°C) were further investigated (Figure S6). The films were found to have disk-like morphology. Notably, the branched edges, also the "active" edges, disappeared at 0°C, further confirming the above proposed mechanism for the thermal expansion deformation. The reversible deformation process by varying temperature can be detected by the observed change of the absorbance intensity at 380 nm (Figure S7). DLS showed the consistent results among the three states (Figure 3F). Therefore, these results confirmed the temperature-adaptive deformation ability of the supramolecular assemblies, which might be potentially applied in smart soft materials (Samanta et al., 2017; Stoffelen et al., 2014; Sankaran et al., 2015).
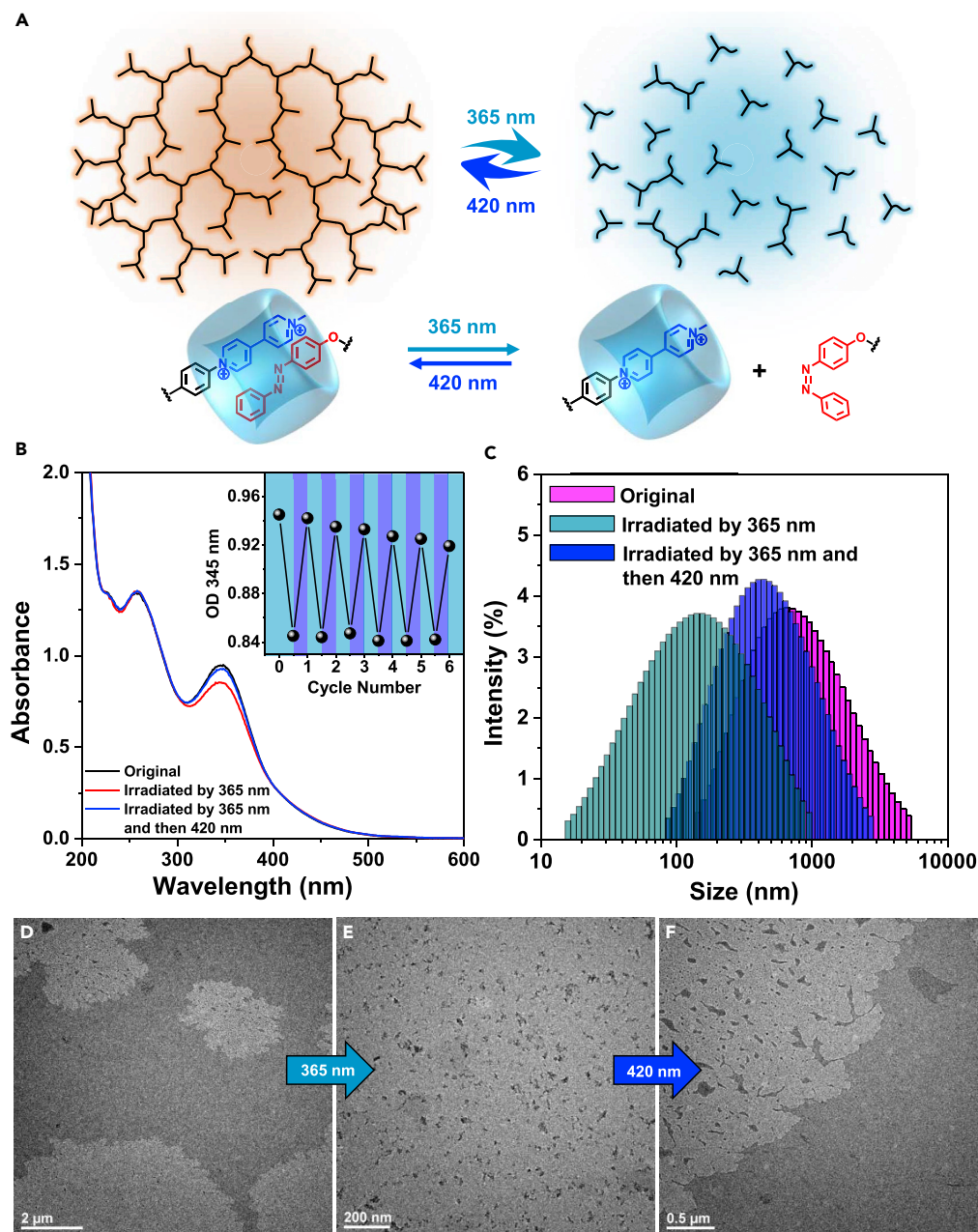
Figure 4. Photo-Induced Disassembly/Reassembly

(A) Schematic representation of the photo-switchable disassembly/reassembly process triggered by the photoisomerization of the azobenzene units.

(B) UV-Vis absorption spectra (50 μM in H_2O) detecting the photo-isomerization process of the azobenzene units. The inset curve shows the reversible switching cycles driven by repeating UV (365 nm, 2 min) and visible light (420 nm, 5 min) irradiation.

(C) DLS results of the supramolecular films before and after corresponding light irradiation.

(D–F) TEM images show the reversible light-switched disassembly/reassembly morphologies.

It is also worthwhile to exploit the photo-degradable or recyclable polymers because of the vital importance of rising energy and environment issues. Owing to the presence of photo-responsive azobenzene units, the supramolecular assemblies also exhibited photo-switchability (Figure 4A). Upon irradiation by UV light (λ = 365 nm), the *trans*-**1** performed typical photo-isomerization into *cis*-form, which had a larger steric hindrance and thus disconnected from the ternary host-guest combination, leading to the

light-induced disassembly of the supramolecular assemblies. The light-switching process was detected by UV-Vis spectra (Figures 4B and S8). The azobenzene absorption peak at 345 nm can be switched reversibly in six cycle times by repeating irradiation of UV light (λ = 365 nm, 2 min) and visible light (λ = 420 nm, 5 min). DLS results showed that the size of assemblies decreased remarkably after irradiation of UV light (Figure 4C), suggesting the efficient disassembly process. TEM and AFM images confirmed that the micrometer-sized supramolecular assemblies (Figures 4D, S9, and S10) were disassembled into small nano-particles (NPs) (Figure 4E), which was consistent with the result measured in DLS (Figure 4C). The visible-light-induced inverse re-assembly process was also confirmed by DLS and TEM images (Figures 4C and 4F). Therefore, these observations indicated the excellent photo-switchability of the resulting supra-molecular assemblies, which might provide new strategies and models for the design and construction of photo-switchable supramolecular materials (Del Barrio et al., 2016).

The porous structure and micrometer size of the supramolecular assemblies enable this materials potential to be used as a filter for NPs. The 2D supramolecular assemblies can be deposited on a commercial poly-ethersulfone (PES) filter with an average pore diameter of 0.22 μm by easily filtering the aqueous solution through the PES filter (Figure 5A). The 0.22-μm pores of the PES filter would selectively make the micro-sized supramolecular films left on the PES film to form a PES-supported supramolecular film. The entrap-ment proportion of the PES filter for the supramolecular assemblies can be evaluated as 8.8% by comparing the relative absorbance at 345 nm before and after filtration (Figure S11). Thus, the immobilized density of the supramolecular film can be evaluated to be 1.42×10^{-9} mol $\cdot$ cm^{-2}. Such immobilization density is quite low compared with the previous examples in NP filter membranes (Krieg et al., 2011). SEM images also showed the well-dispersed 2D assemblies deposited on the PES substrate (Figure S12). Then the filtra-tion capability of the resulting film was tested for gold NPs with different sizes (Figure S13). The filtration process can be performed by simply filtering the NP solution through the film by a syringe (Figures 5B and S14). In the case of 5.5-nm gold NPs, the filtrate was found to be almost colorless (Figures 5C and S15), and the film after filtration turned into red (Figure 5D), indicating the efficient filtration for the gold NPs with small sizes.

The temperature-adaptive capability of the resulting supramolecular assemblies provides possibilities to enable this filtration material with "on-demand" modulable pore sizes (Figure 5E). As the previous demon-stration in Figure 3, the pores of the supramolecular assemblies can be expanded/contracted between about 5 and 40 nm. Hence, we expected that this property could be used for "on-demand" filtration appli-cations, meaning enabling membrane filter materials with "smart" pores, whose diameters could be switched by external stimuli for specific requirements. Quantitative experiments indicated that the depos-ited supramolecular assemblies at 0°C and 25°C exhibited over 90% filtration efficiency for all the tested gold NPs (Figure 5F), which was much higher than that of series of blank control samples especially for NPs with small sizes. These results indicate the excellent performance of the resulting porous supramolec-ular assemblies for NP filtration, and the required film amount for high entrapment proportion is as low as 1.42×10^{-9} mol $\cdot$ cm^{-2}, which represents an advanced membrane filter exhibiting distinct advantages at high entrapment proportion as well as low materials utilization amount. Remarkably, the filter material made by filtering the "expanded" supramolecular assemblies at 40°C through the PES filter showed remarkable decreased filtration efficiency for small NPs of 5.5 and 20 nm, whereas it basically remained high efficiency for large NPs of 60 nm. That indicated the effective regulation of the pore diameters of the supramolecular film filter, showing a distinct adaptiveness of filtration functionality (Geise et al., 2010; Luo et al., 2018; Zhang et al., 2018a, 2018b, 2018c, 2018d; Zou and Zhu, 2018; Wang et al., 2018a, 2018b, 2018c; Zhu et al., 2018; Liang et al., 2018a, 2018b).

Conclusion

In this research, we have demonstrated synthetic 2D supramolecular assemblies that integrate water-sol-ubility, free-standing ability, micrometer size, nanometer thickness, photo-switchability, and dynamic adaptive pore diameters. The distinct semi-rigid structural design not only significantly supports the large area and solubility features of the 2D assemblies but also makes them dynamically adaptive with the external environmental change. This unique adaptive property also enables the 2D assemblies as an "on-demand" filter material that exhibits the intelligence of modulable pore sizes. We expect this concept as a potential origin toward smart 2D materials, which presents that the combination of dynamic supramo-lecular assemblies and 2D materials could provide plenty of new possibilities to construct smart soft 2D materials with more complex functions and applications.
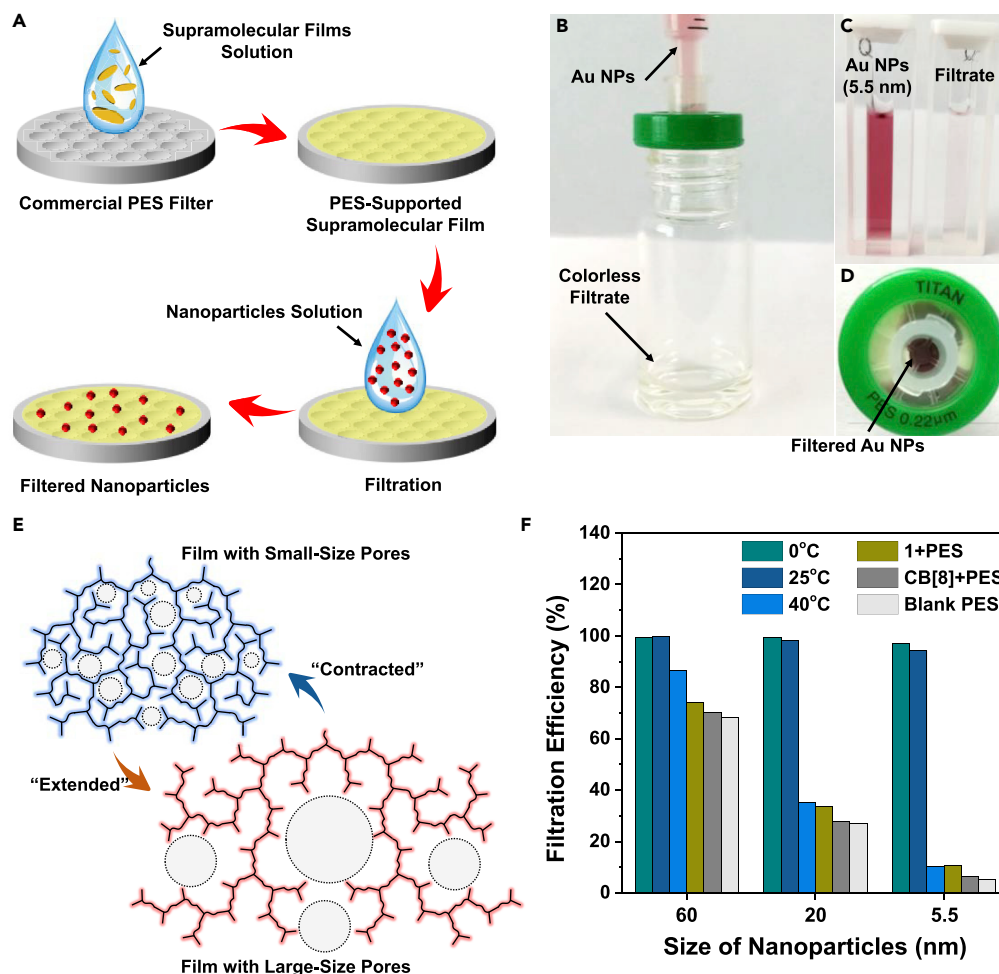
Figure 5. Application in On-Demand Filtration for Nanoparticles

(A) Schematic representation of the preparation of supramolecular filter based on the *trans*-**1**@CB[8] 2D assemblies and its application for separation of NPs.

(B) Photograph shows a supramolecular filter under filtering the 20 nm gold NPs almost quantitatively.

(C) Photograph of the 5.5-nm gold NPs solution before and after filtration.

(D) Top view of a supramolecular filter supported on PES filter after filtering 5.5-nm gold NPs.

(E) Schematic representation of the adaptive capability of the supramolecular film with switchable pore diameters.

(F) Filtration efficiency of the supramolecular film filters prepared under different temperatures (0°C, 25°C, and 40°C) and the three control samples for different sizes of gold NPs. Three control samples include: (1) PES filter pre-filtered with compound *trans*-**1** aqueous solution (1 mM); (2) PES filter pre-filtered with CB[8] aqueous solution (0.25 mM); (3) PES filter without any pre-filtration.

Limitations of the Study

This research provides a distinct structural design strategy for 2D supramolecular assemblies based on host-guest combinations. However, the poor water solubility of macrocycle CB[8] limits the water solubility of the resulting assemblies in only 1 mM scale, which is not high enough for further processing and applications. Moreover, the multi-step synthesis of monomers and macrocycles makes the material costly. Hence, functional materials made by easier and cheaper method should be exploited in future research.

METHODS

All methods can be found in the accompanying Transparent Methods supplemental file.

AUTHOR CONTRIBUTIONS

Q.Z. and D.-H.Q. conceived the project and designed the experiments. R.-J.X. and W.-Z.W. performed the synthetic experiments. Q.Z. and R.X. carried out material characterization. Y.-X.D. assisted in material characterization. Q.Z., D.H.Q., and H.T. wrote the manuscript. All authors discussed the results and commented on the manuscript.

DECLARATION OF INTERESTS

The authors declare no competing interests.

REFERENCES

Amabilino, D.B., Smith, D.K., and Steed, J.W. (2017). Supramolecular materials. Chem. Soc. Rev. *46*, 2404–2420.

Appel, E.A., del Barrio, J., Loh, X.J., and Scherman, O.A. (2012). Supramolecular polymeric hydrogels. Chem. Soc. Rev. *41*, 6195–6214.

Baek, K., Yun, G., Kim, Y., Kim, D., Hota, R., Hwang, I., Xu, D., Ko, Y.H., Gu, G.H., Suh, J.H., et al. (2013). Free–standing, single–monomer–thick two–dimensional polymers through covalent self–assembly in solution. J. Am. Chem. Soc. *135*, 6523–6528.

Del Barrio, J., Horton, P.N., Lairez, D., Lloyd, G.O., Toprakcioglu, C., and Scherman, O.A. (2013). Photocontrol over Cucurbit[8]uril complexes: stoichiometry and supramolecular polymers. J. Am. Chem. Soc. *135*, 11760–11763.

Del Barrio, J., Ryan, S.T.J., Jambrina, P.G., Rosta, E., and Scherman, O.A. (2016). Light–regulated molecular trafficking in a synthetic water–soluble host. J. Am. Chem. Soc. *138*, 5745–5748.

Barrow, S.J., Kasera, S., Rowland, M.J., del Barrio, J., and Scherman, O.A. (2015). Cucurbituril–based molecular recognition. Chem. Rev. *115*, 12320–12406.

Chen, Y., and Liu, Y. (2015). Construction and functions of cyclodextrin–based 1d supramolecular strands and their secondary assemblies. Adv. Mater. *27*, 5403–5409.

Chen, L., Xiang, J., Zhao, Y., and Yan, Q. (2018). Reversible self–assembly of supramolecular vesicles and nanofibers driven by chalcogen–bonding interactions. J. Am. Chem. Soc. *140*, 7079–7082.

Cohen, E., Weissman, H., Pinkas, I., Shimoni, E., Rehak, P., Král, P., and Rybtchinski, B. (2018). Controlled self–assembly of photofunctional supramolecular nanotubes. ACS Nano *12*, 317–326.

Colson, J.W., and Dichtel, W.R. (2013). Rationally synthesized two–dimensional polymers. Nat. Chem. *5*, 453–465.

Datta, S., Misra, S.K., Saha, M.L., Lahiri, N., Louie, J., Pan, D., and Stang, P.J. (2018). Orthogonal self–assembly of an organoplatinum(II) metallacycle and cucurbit[8]uril that delivers curcumin to cancer cells. Proc. Natl. Acad. Sci. U S A *115*, 8087–8092.

Dong, S.-Y., Luo, Y., Yan, X.-Z., Zheng, B., Ding, X., Yu, Y.-H., Ma, Z., Zhao, Q.-L., and Huang, F.-H. (2011a). A dual–responsive supramolecular polymer gel formed by crown ether based molecular recognition. Angew. Chem. Int. Ed. *50*, 1905–1909.

Dong, R.-J., Liu, Y., Zhou, Y.-F., Yan, D.-Y., and Zhu, X.-Y. (2011b). Photo–Reversible supramolecular hyperbranched polymer based on host–guest interactions. Polym. Chem. *2*, 2771–2774.

Dong, R.-J., Zhou, Y.-F., and Zhu, X.-Y. (2014). Supramolecular dendritic polymers: from synthesis to applications. Acc. Chem. Res. *47*, 2006–2016.

Dong, R.-H., Zhang, T., and Feng, X.-L. (2018). Interface-assisted synthesis of 2D materials: trend and challenges. Chem. Rev. *118*, 6189–6235.

Fang, R.-C., Liu, Y.-L., Wang, Z.-Q., and Zhang, X. (2013). Water–soluble supramolecular hyperbranched polymers based on host–enhanced π–π interaction. Polym. Chem. *4*, 900–903.

Fernández, G., Pérez, E.M., Sánchez, L., and Martín, N. (2008). An electroactive dynamically polydisperse supramolecular dendrimer. J. Am. Chem. Soc. *130*, 2410–2411.

Gaitzsch, J., Huang, X., and Voit, B. (2016). Engineering functional polymer capsules toward smart nanoreactors. Chem. Rev. *116*, 1053–1093.

Gao, C., Huang, Q.-X., Lan, Q.-P., Feng, Y., Tang, F., Hoi, M.P.M., Zhang, J.-X., Lee, S.M.Y., and Wang, R.-B. (2018). A user–friendly herbicide derived from photo–responsive supramolecular vesicles. Nat. Commun. *9*, 2967.

Geise, G.M., Lee, H.S., Miller, D.J., Freeman, B.D., McGrath, J.E., and Paul, D.R. (2010). Water purification by membranes: the role of polymer science. J. Polym. Sci. Pol. Phys. *48*, 1685–1718.

Groombridge, A.S., Palma, A., Parker, R.M., Abell, C., and Scherman, O.A. (2017). Aqueous

interfacial gels assembled from small molecule supramolecular polymers. Chem. Sci. 8, 1350–1355.

Hendricks, M.P., Sato, K., Palmer, L.C., and Stupp, S.I. (2017). Supramolecular assembly of peptide amphiphiles. Acc. Chem. Rev. 50, 2440–2448.

Hu, C.-H., Ma, N.-N., Li, F., Fang, Y., Liu, Y., Zhao, L.-L., Qiao, S.-P., Li, X.-M., Jiang, X.-J., Li, T.-Z., et al. (2018). Cucurbit[8]uril–based giant supramolecular vesicles: highly stable, versatile carriers for photoresponsive and targeted drug delivery. ACS Appl. Mater. Interfaces 10, 4603–4613.

Huang, F., and Gibson, H.W. (2004). Formation of a supramolecular hyperbranched polymer from self–organization of an AB2 monomer containing a crown ether and two paraquat moieties. J. Am. Chem. Soc. 126, 14738–14739.

Ji, X.-F., Wu, R.-T., Long, L.-L., Ke, X.-S., Guo, C.-X., Ghang, Y.-J., Lynch, V.M., Huang, F.-H., and Sessler, J.L. (2018). Encoding, reading, and transforming information using multifluorescent supramolecular polymeric hydrogels. Adv. Mater. 30, 1705480.

Jones, C.D., and Steed, J.W. (2016). Gels with sense: supramolecular materials that respond to heat, light and sound. Chem. Soc. Rev. 45, 6546–6596.

Krieg, E., Weissman, H., Shirman, E., Shimoni, E., and Rybtchinski, B. (2011). A recyclable supramolecular membrane for size-selective separation of nanoparticles. Nat. Nanotechnol. 6, 141–146.

Krieg, E., Bastings, M.M.C., Besenius, P., and Rybtchinski, B. (2016). Supramolecular polymers in aqueous media. Chem. Rev. 116, 2414–2477.

Liang, B., Wang, H., Shi, X.-H., Shen, B.-Y., He, X., Ghazi, Z.A., Khan, N.A., Sin, H., Khattak, A.M., Li, L.-S., et al. (2018a). Microporous membranes comprising conjugated polymers with rigid backbones enable ultrafast organic–solvent nanofiltration. Nat. Chem. 10, 961–967.

Liang, B., He, X., Hou, J.-J., Li, L.-S., and Tang, Z.-Y. (2018b). Membrane separation in organic liquid: technologies, achievements, and opportunities. Adv. Mater. e1806090.

Liu, T.-T., Wang, S.-D., Li, Y.-R., Yan, H.-X., and Tian, W. (2018). Triple noncovalent–interaction–containing supramolecular polymer vesicle chemosensors with dynamically tunable detection ranges. Chem. Eur. J. 24, 4239–4244.

Luo, H.-X., Aboki, J., Ji, Y.-Y., Guo, R.-L., and Geise, G.M. (2018). Water and salt transport properties of triptycene–containing sulfonated polysulfone materials for desalination membrane applications. ACS Appl. Mater. Interfaces 10, 4102–4112.

Lutz, J.-F., Lehn, J.M., Meijer, E.W., and Matyjaszewski, K. (2016). From precision polymers to complex materials and systems. Nat. Rev. Mater. 1, 16024.

Matsumoto, M., Valentino, L., Stiehl, G.M., Balch, H.B., Corcos, A.R., Wang, F., Ralph, D.C., Marinas, B.J., and Dichtel, W.R. (2018). Lewis–

acid–catalyzed interfacial polymerization of covalent organic framework films. Chem 4, 308–317.

Pazos, E., Novo, P., Peinador, C., Kaifer, A.E., and García, M.D. (2019). Cucurbit[8]uril (CB[8]) –based supramolecular switches. Angew. Chem. Int. Ed. 58, 403–416.

Pfeffermann, M., Dong, R.-H., Graf, R., Zajaczkowski, W., Gorelik, T., Pisula, W., Narita, A., Müllen, K., and Feng, X.-L. (2015). Free–standing monolayer two–dimensional supramolecular organic framework with good internal order. J. Am. Chem. Soc. 137, 14525–14532.

Qu, D.-H., Wang, Q.-C., Zhang, Q.-W., Ma, X., and Tian, H. (2015). Photoresponsive host–guest functional systems. Chem. Rev. 115, 7543–7588.

Samanta, S.K., Quigley, J., Vinciguerra, B., Briken, V., and Isaacs, L. (2017). Cucurbit[7]uril enables multi–stimuli–responsive release from the self–assembled hydrophobic phase of a metal organic polyhedron. J. Am. Chem. Soc. 139, 9066–9074.

Sankaran, S., Kiren, M.C., and Jonkheijm, P. (2015). Incorporating bacteria as a living component in supramolecular self–assembled monolayers through dynamic nanoscale interactions. ACS Nano 9, 3579–3586.

Stoffelen, C., Voskuhl, J., Jonkheijm, P., and Huskens, J. (2014). Dual stimuli–responsive self–assembled supramolecular nanoparticles. Angew. Chem. Int. Ed. 53, 3400–3404.

Sun, B., Kim, Y., Wang, Y.-Q., Wang, H.-X., Kim, J., Liu, X., and Lee, M. (2018). Homochiral porous nanosheets for enantiomer sieving. Nat. Mater. 17, 599–604.

Tao, W., Liu, Y., Jiang, B.-B., Yu, S.-R., Huang, W., Zhou, Y.-F., and Yan, D.-Y. (2012). A linear–hyperbranched supramolecular amphiphile and its self–assembly into vesicles with great ductility. J. Am. Chem. Soc. 134, 762–764.

Tao, R., Zhang, Q., Rao, S.-J., Zheng, X.-L., Li, M., and Qu, D. (2019). Supramolecular gelator based on a [c2]daisy chain rotaxane: efficient gel-solution transition by ring-sliding motion. Sci. China Chem. 62, 245–250.

Tian, F., Jiao, D.-Z., Biedermann, F., and Scherman, O.A. (2012). Orthogonal switching of a single supramolecular complex. Nat. Commun. 3, 1207.

Tian, J., Zhou, T.-Y., Zhang, S.-C., Aloni, S., Altoe, M.V., Xie, S.-H., Wang, H., Zhang, D.-W., Zhao, X., Liu, Y., et al. (2014). Three–dimensional periodic supramolecular organic framework ion sponge in water and microcrystals. Nat. Commun. 5, 5574.

Tian, W., Li, X.-X., and Wang, J.-X. (2017). Supramolecular hyperbranched polymers. Chem. Commun. 53, 2531–2542.

Voorhaar, L., and Hoogenboom, R. (2016). Supramolecular polymer networks: hydrogels and bulk materials. Chem. Soc. Rev. 45, 4013–4031.

Wang, Y.-K., Yang, Z.-S., Lv, X.-Q., Yao, R.-S., and Wang, F. (2014). Construction of supramolecular hyperbranched polymers via the "tweezering

directed self–assembly" strategy. Chem. Commun. 50, 9477–9480.

Wang, W.-Z., Gao, C., Zhang, Q., Ye, X.-H., and Qu, D.-H. (2017). Supramolecular helical nanofibers formed by achiral monomers and their reversible sol–gel transition. Chem. Asian J. 12, 410–414.

Wang, X.-Y., Chen, L.-J., Chong, S.Y., Little, M.A., Wu, Y.-Z., Zhu, W.-H., Clowes, R., Yan, Y., Zwijnenburg, M.A., Sprick, R.S., et al. (2018a). Sulfone–containing covalent organic frameworks for photocatalytic hydrogen evolution from water. Nat. Chem. 10, 1180–1189.

Wang, Q., Tian, L., Xu, J.-Z., Xia, B., Li, J., Lu, F., Lu, X.-M., Wang, W.-J., Huang, W., and Fan, Q.-L. (2018b). Multifunctional supramolecular vesicles for combined photothermal/photodynamic/hypoxia-activated chemotherapy. Chem. Commun. 54, 10328–10331.

Wang, P.-F., Wang, M., Liu, F., Ding, S.-Y., Wang, X., Du, G.-H., Liu, J., Apel, P., Kluth, P., Trautmann, C., et al. (2018c). Ultrafast ion sieving using nanoporous polymeric membranes. Nat. Commun. 9, 569.

Wang, H., Zeng, Z.-H., Xu, P., Li, L.-S., Zeng, G.-M., Xiao, R., Tang, Z.-Y., Huang, D.-L., Tang, L., Lai, C., et al. (2019). Recent progress in covalent organic framework thin films: fabrications, applications and perspectives. Chem. Soc. Rev. 48, 488–516.

Xiao, P., Bu, F., Zhao, R., Aboud, M.F.A., Shakir, I., and Xu, Y. (2018). Sub-5 nm ultrasmall metal–organic framework nanocrystals for highly efficient electrochemical energy storage. ACS Nano 12, 3947–3953.

Xing, P.-Y., Phua, S.Z.F., Wei, X., and Zhao, Y.-L. (2018). Programmable multicomponent self–assembly based on aromatic amino acids. Adv. Mater. 30, e1805175.

Yagai, S., Kitamoto, Y., Datta, S., and Adhikari, B. (2019). Supramolecular polymers capable of controlling their topology. Acc. Chem. Res. 52, 1325–1335.

Yang, L.-L., Tan, X.-X., Wang, Z.-Q., and Zhang, X. (2015). Supramolecular polymers: historical development, preparation, characterization, and functions. Chem. Rev. 115, 7196–7239.

Yu, G.-C., Jie, K.-C., and Huang, F.-H. (2015). Supramolecular amphiphiles based on host–guest molecular recognition motifs. Chem. Rev. 115, 7240–7303.

Yu, Q.-L., Zhang, Y.-M., Liu, Y.-H., Xu, X., and Liu, Y. (2018). Magnetism and photo dual–controlled supramolecular assembly for suppression of tumor invasion and metastasis. Sci. Adv. 4, eaat2297.

Yue, L., Wang, S., Zhou, D., Zhang, H., Li, B., and Wu, L. (2016). Flexible single–layer ionic organic–inorganic frameworks towards precise nano–size separation. Nat. Commun. 7, 10742.

Zhang, K.-D., Tian, J., Hanifi, D., Zhang, Y., Sue, A.C., Zhou, T.-Y., Zhang, L., Zhao, X., Liu, Y., and Li, Z.-T. (2013). Toward a single–layer two–dimensional honeycomb supramolecular organic framework in water. J. Am. Chem. Soc. 135, 17913–17918.

Zhang, Q., Rao, S.-J., Xie, T., Li, X., Xu, T., Li, D.-W., Qu, D.-H., Long, Y.-T., and Tian, H. (2018a). Muscle-like artificial molecular actuators for nanoparticles. Chem 4, 2670–2684.

Zhang, Y.-M., Zhang, N.-Y., Xiao, K., Yu, Q., and Liu, Y. (2018b). Photo–controlled reversible microtubule assembly mediated by cyclodextrin derivative. Angew. Chem. Int. Ed. 57, 8649–8653.

Zhang, Q., Shi, C.-Y., Qu, D.-H., Long, Y.-T., Feringa, B.L., and Tian, H. (2018c). Exploring a naturally tailored small molecule for stretchable, self–healing, and adhesive supramolecular polymers. Sci. Adv. 4, eaat8192.

Zhang, W.-F., Liu, N., Zhang, Q.-D., Qu, R.-X., Liu, Y.-N., Li, X.-Y., Wei, Y., Feng, L., and Jiang, J. (2018d). Thermo–driven controllable emulsion separation by a polymer–decorated membrane with switchable wettability. Angew. Chem. Int. Ed. 57, 5740–5745.

Zhou, Y.-F., Huang, W., Liu, J.-Y., Zhu, X.-Y., and Yan, D.-Y. (2010). Self–assembly of hyperbranched polymers and its biomedical applications. Adv. Mater. 22, 4567–4590.

Zhu, J.-Y., Hou, J.-W., Uliana, A., Zhang, Y.-T., Tian, M.-M., and van der Bruggen, B. (2018). The rapid emergence of two–dimensional nanomaterials for high–performance separation membranes. J. Mater. Chem. A 6, 3773–3792.

Zhuang, X.-D., Mai, Y.-Y., Wu, D.-Q., Zhang, F., and Feng, X.-L. (2015). Two–Dimensional soft nanomaterials: a fascinating world of materials. Adv. Mater. 27, 403–427.

Zou, X.-Q., and Zhu, G.-S. (2018). Microporous organic materials for membrane–based gas separation. Adv. Mater. 30, 1700750.

Supplemental Information

Dynamic Adaptive Two-Dimensional

Supramolecular Assemblies

for On-Demand Filtration

Qi Zhang, Ruo-Jie Xing, Wen-Zhi Wang, Yuan-Xin Deng, Da-Hui Qu, and He Tian

Supplementary Information

CONTENT:

1. Transparent Method

2. Synthetic Procedures

3. Supporting Figures

1. Transparent Method

All the reagents were used as received from Adamas®beta, Aladdin and Aldrich. All organic solvents were reagent grade and were dried and distilled prior to use according to standard procedures. Ultrapure water (18.2 MΩ cm) was obtained from a Millipore system (Labconco Corporation, Kansas City, MO, U.S.A). The synthetic products were characterized by ^{1}H NMR, ^{13}C NMR spectroscopies and high resolution electronic spray ionization (ESI) mass spectrometry to confirm the molecular structures. ^{1}H NMR and ^{13}C NMR were obtained from Brüker AV-400 spectrometer employing tetramethylsilane as the internal standard. The ESI mass spectra were acquired on an LCT Premier XE mass spectrometer. UV-Vis absorption spectra were recorded on an Agilent Cary 100 spectrometer (1 cm quartz cells if no specialized note). Dynamic light scattering (DLS) was measured on Beckman Coulter DelsaNano C, 298 K. The morphology of the nano-assemblies was detected on high resolution transmission electron microscopy (HR-TEM) from JEM-1400, JEOL. The sample solutions were dropped onto a copper grid with carbon membrane and evaporated in vacuum oven at corresponding temperature. Surface morphology images of samples were detected by atomic force microscopy (AFM) from Veeco/DI. The sample solution were dropped on a freshly peeled mica sheet and evaporated in vacuum oven at corresponding temperature. The photo-irradiation experiments were performed in a quartz cell under the UV/visible irradiation of a high-power LED lamp with single wavelength output (365 nm or 420 nm), PL-LED100, PerfectLight®. The output power was set as 30 W and the distance between quartze cell and light source was 2 cm. The nanoparticle filter experiments were performed based on the commercial polyethersulfone (PES) filter (Adamas®beta) with average pore diameter of 0.22 μm. The filtration efficiency was calculated based on the relative concentration ratio of the samples before and after filtered, which was required by the relative absorbance at the UV-Vis absorption peaks.

2. Synthetic procedures
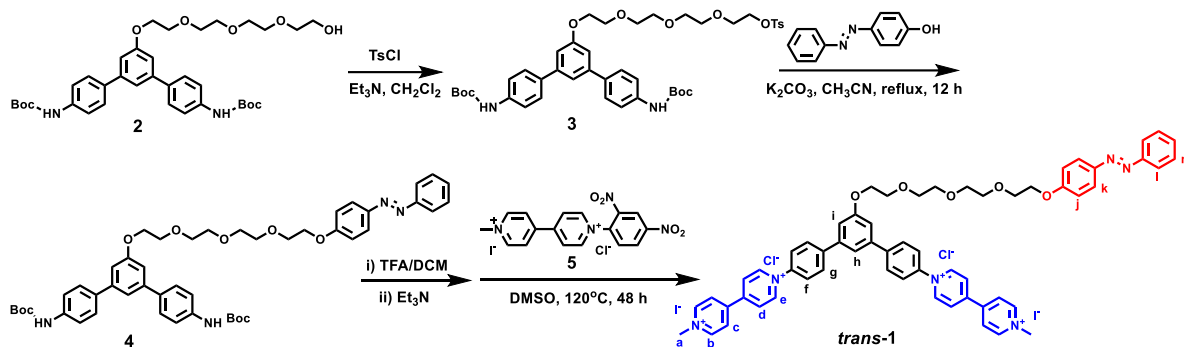
Preparation of compound 3: The compound **2** (1.711 g, 2.61 mmol) and p-toluenesulfonyl chloride (0.900 g, 4.72 mmol) were dissolved in CH_2Cl_2 (10 mL). Then, TEA (1 mL) was added into the solution. After stirring for 6 hours at room temperature, the precipitate was removed through filtration, and the filtrate was evaporated. The crude product was purified by chromatography on a silica gel column (PE/EA = 1/1) to yield the compound **3** (1.724 g, 81.6%) as a yellow oily liquid. ^{1}H NMR (400 MHz, CDCl3) δ (ppm): 7.786 (d, J = 8.4 Hz, 2H), 7.558 (d, J = 8.4 Hz, 4H), 7.445 (d, J = 8.4z, 4H), 7.320 (t, 3H), 7.055 (s, 2H), 6.559 (s, 2H), 4.247 (t, J = 4.8 Hz, 2H), 4.144 (t, J = 4.8, 2H), 3.901 (t, J = 4.8 Hz, 2H), 3.743 (m, 2H), 3.674 (m, 4H), 3.586 (m, 4H), 2.416 (s, 3H), 1.534 (s, 18H). ^{13}C NMR (100 M Hz, CDCl3) δ 159.5, 152.7, 144.8, 142.4, 138.0, 135.6, 132.9, 129.8, 128.0, 127.7, 118.7, 118.2, 111.7, 80.6, 70.8, 70.7, 70.7, 70.6, 69.8, 69.3, 68.7, 67.6, 28.4, 21.6. HRMS (ESI) (m/z): [M + Na][+] calcd for $C_{43}H_{54}N_2O_{11}SNa$: 829.3346, found: 829.3369.

Preparation of compound 4: The compound **3** (1.724 g, 2.14 mmol) and p-hydroxyazobenzene (0.508 g, 2.56 mmol) were dissolved in CH_3CN (10 mL) with K_2CO_3 (0.885 g, 6.42 mmol) added in it afterwards. The mixture was refluxed for 12 hours. After the precipitate was filtered and the solvent was evaporated, the crude product was further purified by chromatography on a silica gel column (PE/EA = 1/1) to yield the compound **3** (1.236 g, 69.3%) as a red oily liquid. ^{1}H NMR (400 M Hz, CDCl3) δ (ppm): 7.889 (m, 4H), 7.550-7.431 (m, 11H), 7.314 (s, 1H), 7.055 (s, 2H), 7.007 (d, J = 8.8 Hz, 2H), 6.568 (s, 2H), 4.245 (m, 2H), 4.189-3.908 (m, 6H), 3.766-3.694 (m, 8H), 1.528 (s, 18H). ^{13}C NMR (100 M Hz, CDCl3) δ

171.2, 161.3, 159.5, 152.8, 142.5, 138.0, 135.7, 130.4, 129.8, 129.0, 128.0, 127.7, 124.7, 122.6, 118.8, 114.8, 111.7, 80.6, 70.9, 70.7, 69.8, 69.6, 69.3, 68.7, 67.6, 60.4, 28.4. HRMS (ESI) (m/z): $[M + Na]^+$ calcd for $C_{48}H_{56}N_4O_9Na$: 855.3945, found: 855.3942.

Preparation of compound *trans*-1: The compound **4** (300 mg, 0.36 mmol) was dissolved in CH_2Cl_2 (5.0 mL) and then trifluoroacetic acid (0.412 g, 3.6 mmol) was added and the mixture was stirred for 4 hours. After the removal of the solution, triethylamine (2 mL) was added to deprotonate the amino groups. Dissolved in CH_2Cl_2, the mixture was washed with water (3 × 20 mL). The combined organic layers were dried over Na_2SO_4 and concentrated under reduced pressure to yield some red oily liquid. Then, it was dissolved with **5** (364 mg, 0.727 mmol) in DMSO (3 mL) and stirred at 120℃ for 2 days. The mixture was added into acetone (150 mL), and the result powder was filtered, washed by hot acetone (3 × 60 mL), and recrystallized in EtOH/H_2O twice to yield the compound **4** (89 mg, 19.5%) as a dark red solid. ^1H NMR (400 M Hz, D_2O) δ (ppm): 9.311 (d, J = 7.2 Hz, 4H), 9.086 (d, J = 6.8 Hz, 4H), 8.667 (d, J = 6.8 Hz, 4H), 8.564 (d, J = 6.8 Hz, 4H), 8.045 (d, J = 8.8 Hz, 4H), 7.859 (d, J = 8.8 Hz, 4H), 7.680 (s, 1H), 7.535 (m, 4H), 7.393 (m, 5H), 6.865 (d, J = 9.2 Hz, 2H), 4.524 (s, 6H), 4.390 (t, J = 4.4 Hz, 2H), 4.039 (t, J = 4.0 Hz, 2H), 3.935 (t, J = 4.0 Hz, 2H), 3.863 (t, J = 3.2 Hz, 2H), 3.783 (m, 2H), 3.734 (m, 4H), 3.688 (m, 2H). ^{13}C NMR (600 M Hz, DMSO-d_6) δ 161.7, 160.3, 152.4, 151.5, 149.7, 148.2, 147.2, 146.3, 145.8, 143.2, 142.1, 140.9, 131.3, 129.9, 129.2, 126.9, 126.8, 125.8, 125.0, 122.7, 122.6, 115.5, 70.5, 70.4, 70.4, 70.3, 69.5, 69.3, 68.1, 68.1, 48.6. HRMS (ESI) (m/z): $[M - 2I]^{2+}$ calcd for $C_{60}H_{58}N_6O_5Cl_2$: 506.1917, found: 506.1910.

2. Supporting Figures
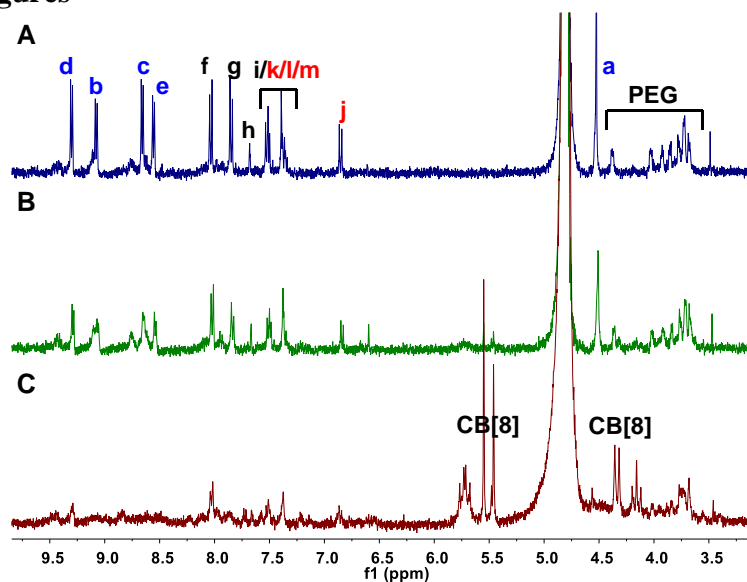
Figure S1. ^{1}H NMR titration experiments (D$_2$O, 400 MHz, 298K), related to Figure 2. (a) *trans*-**1**, (b) *trans*-**1** + CB[8] (1 : 0.75), (c) *trans*-**1** + CB[8] (1 : 1.5). Concentration of *tran*-**1** was 1 mM.
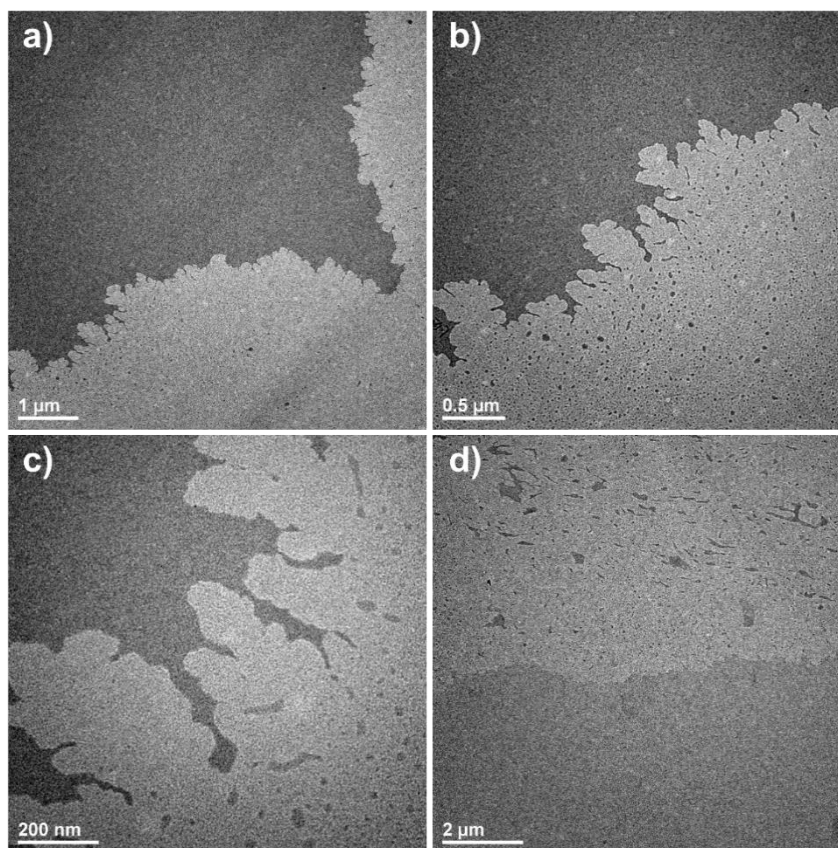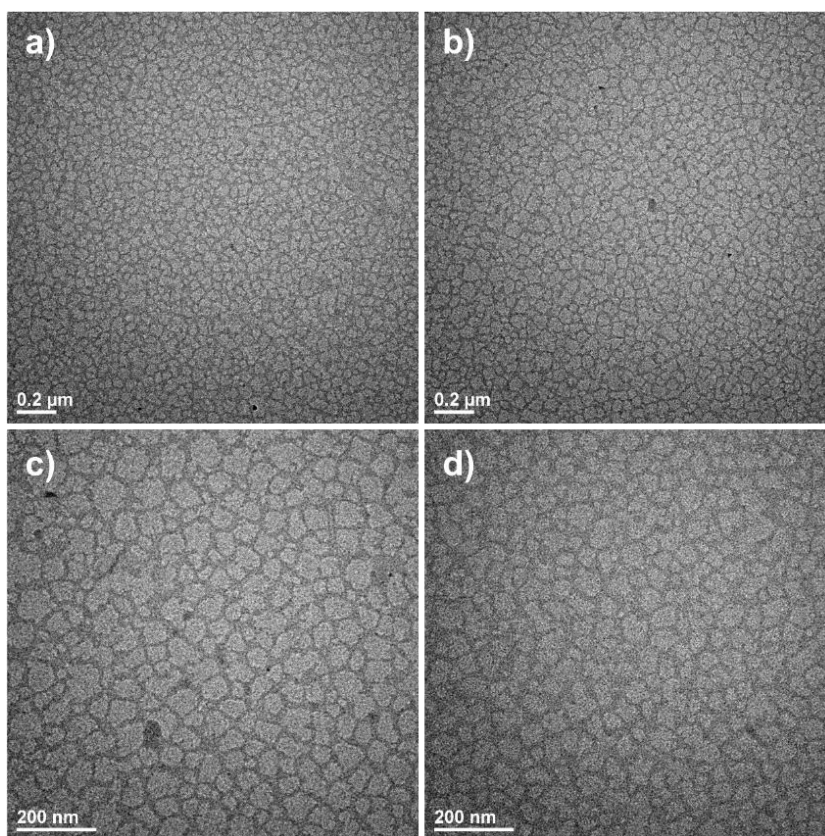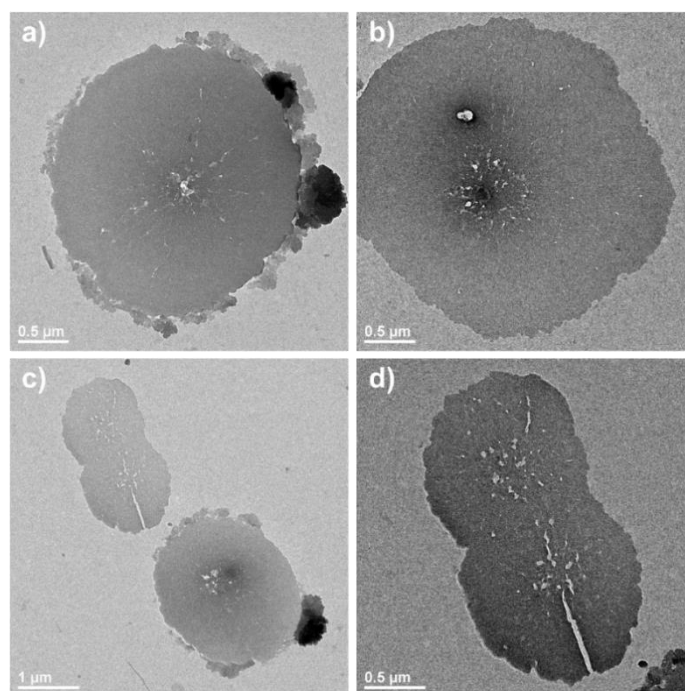

Figure S2. TEM images with different magnifications of the resulting supramolecular films, related to Figure 2.
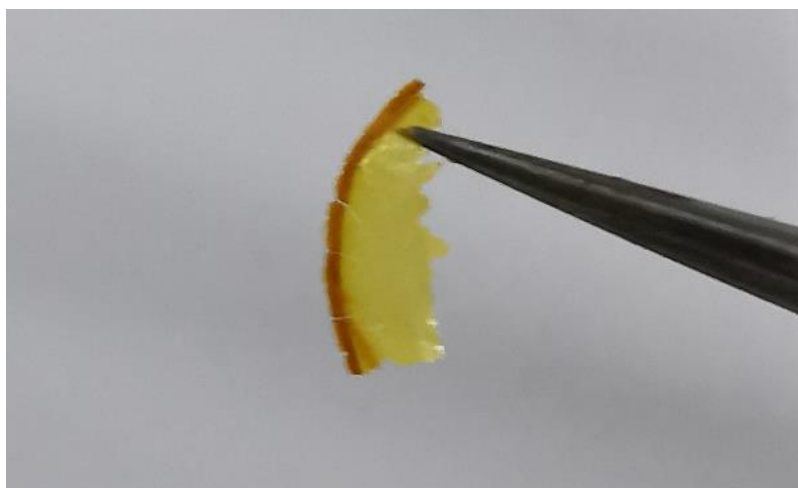
Figure S3. Photograph shows the free-standing film prepared by drop-casting method of the supramolecular assemblies solution, related to Figure 2.
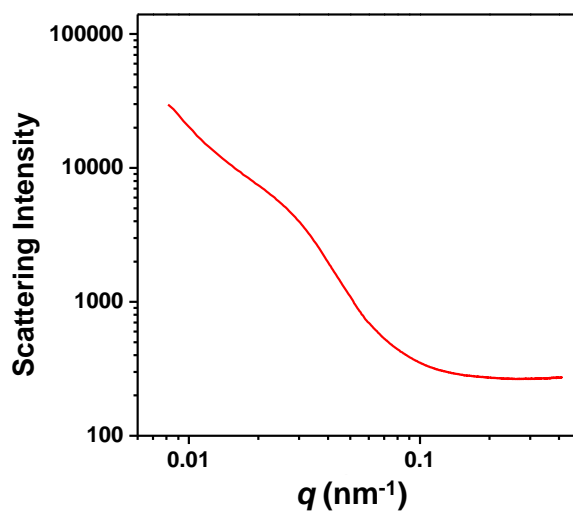
Figure S4. Synchrotron radiation SAXS pattern of the resulting supramolecular films, related to Figure 2.

Figure S5. TEM images with different magnifications of the resulting supramolecular films at high temperature (40ºC), related to Figure 3.

Figure S6. TEM images with different magnifications of the resulting supramolecular films at low temperature (0ºC), related to Figure 3.
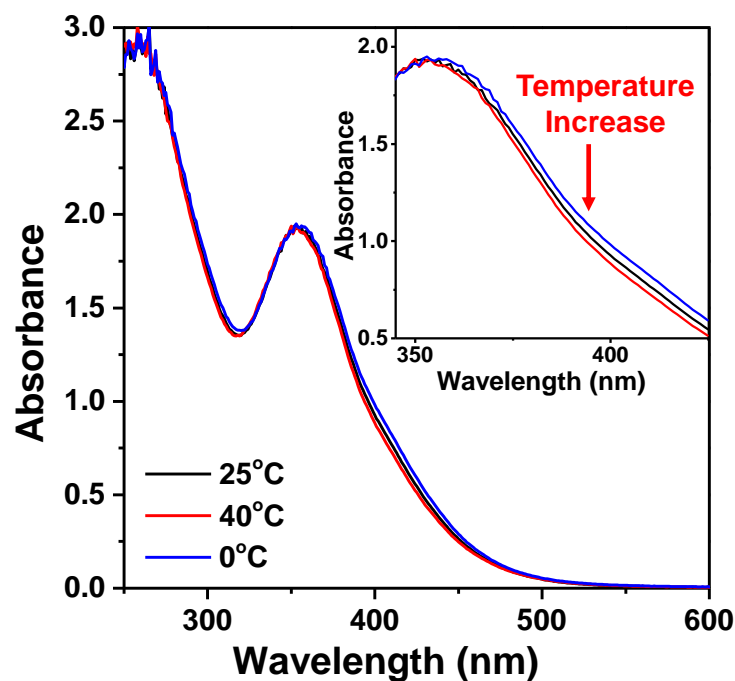
Figure S7. UV-Vis absorption spectra of the supramolecular polymers *trans*-1@CB[8] solution (1 mM, H₂O) under different temperature, related to Figure 3. Cuvette with short path length (1 mm) was used in this experiment due to the high concentration of solutes. The inset spectra show the amplified curve shifts at varied temperature.
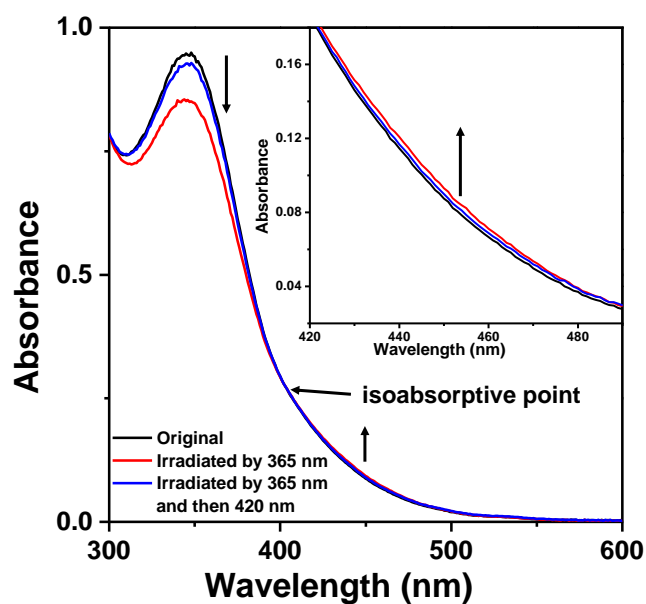
Figure S8. UV-Vis absorption spectra (50 μM in H₂O) detecting the photo-isomerization process of the azobenzene units, related to Figure 4. The inset image shows the amplified region of the increasing absorbance attributed to the *cis*-azobenzene.
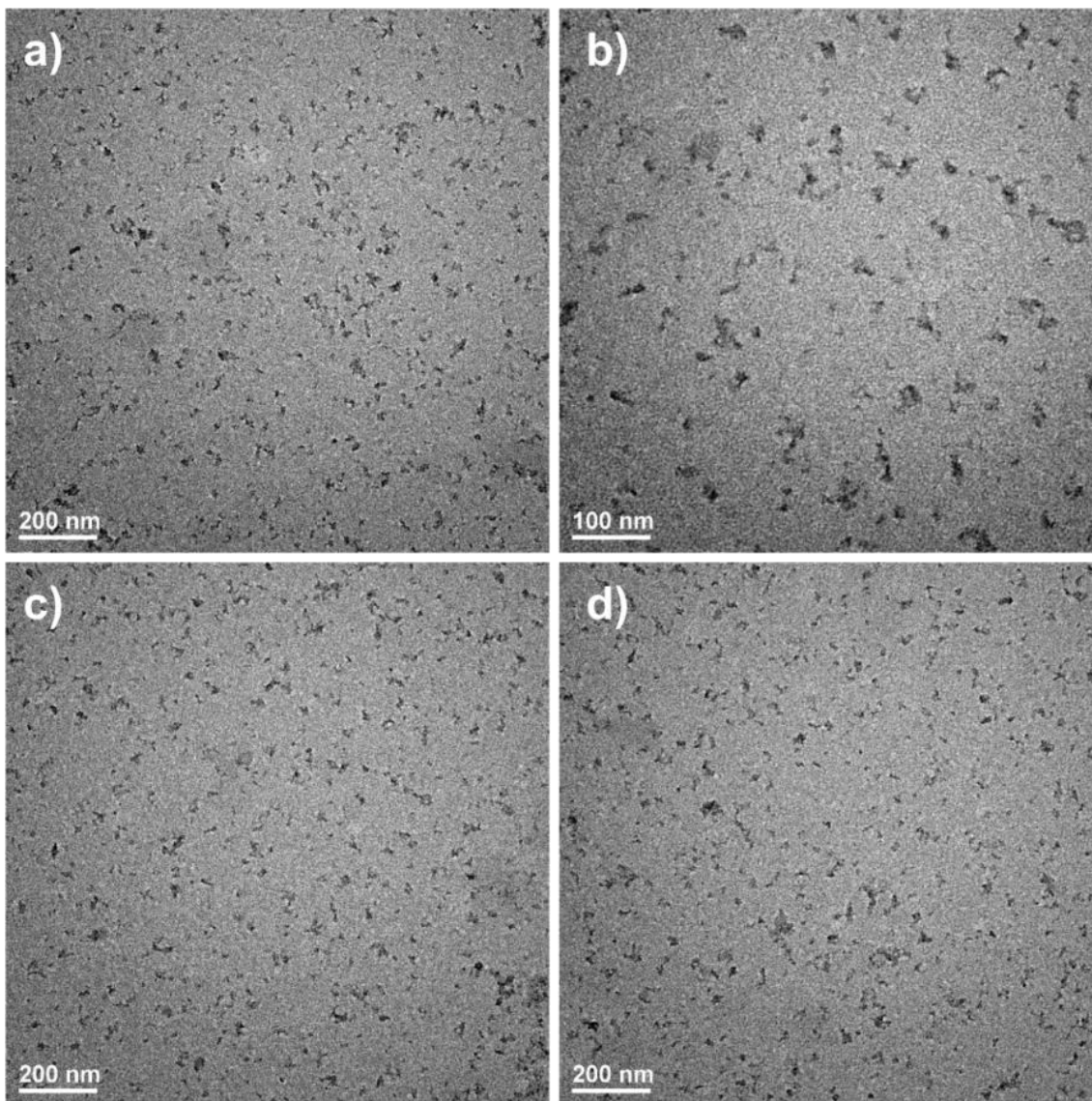
Figure S9. TEM images of the UV-induced disassemblies, related to Figure 4.
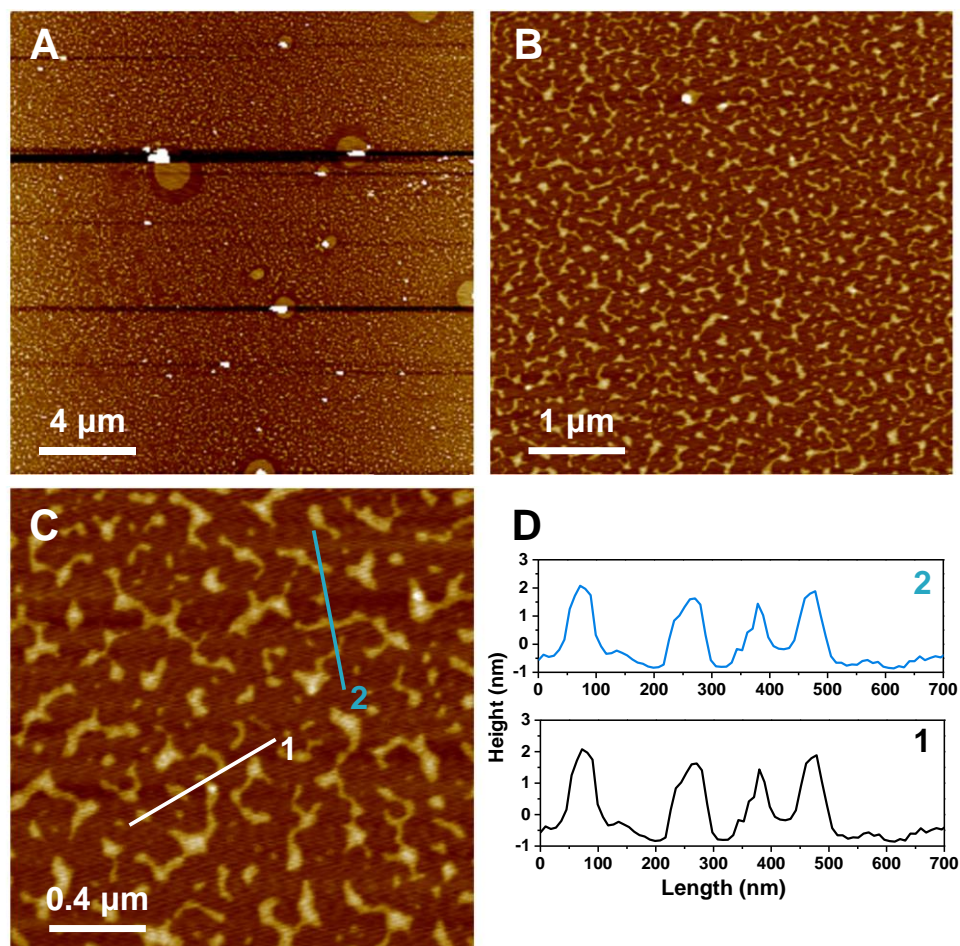
Figure S10. AFM images of the UV-induced disassemblies, related to Figure 4.
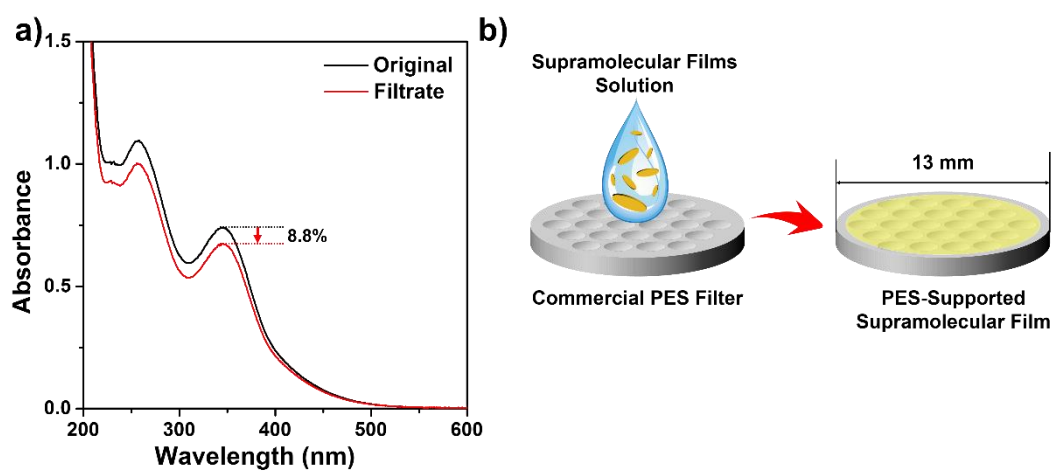
Figure S11. UV-Vis absorption spectra of the supramolecular film solution before and after filtrated by PES filter, related to Figure 5. The original concentration was 0.33 mM. The volume was 1 mL. Scheme of the filtration process (b). The diameter of the PES substrate was 13 mm.
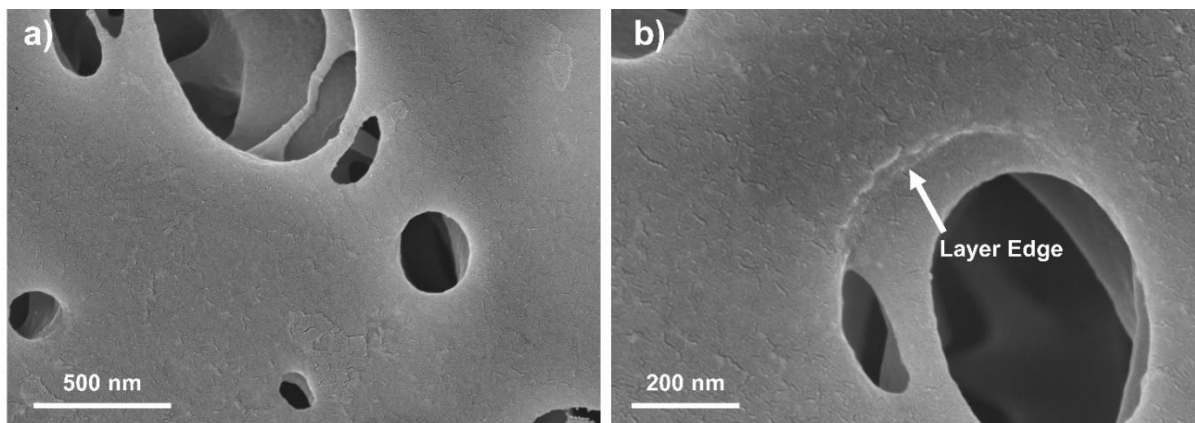
Figure S12. SEM images of the 2D network attached on the PES filter, related to Figure 5. The visible pores with hundreds of nanometers belong to the PES filter. A visible layer edge is showed in a higher magnification (b), showing the nano-sized thickness of the layered 2D network. Images with the larger amplification times are not available because of the instability of the 2D network under high-energy electron beam.
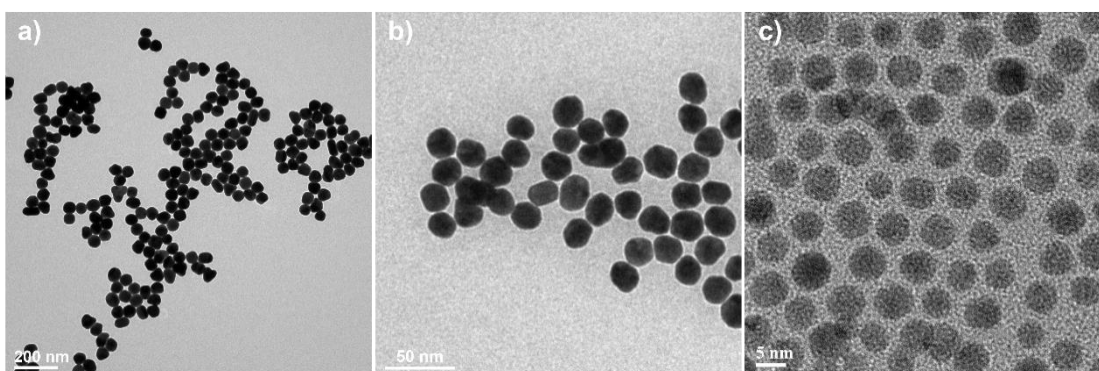
Figure S13. TEM images of the tested gold NPs with different sizes, related to Figure 5. (a) 60 nm; (b) 20 nm; (c) 5.5 nm.
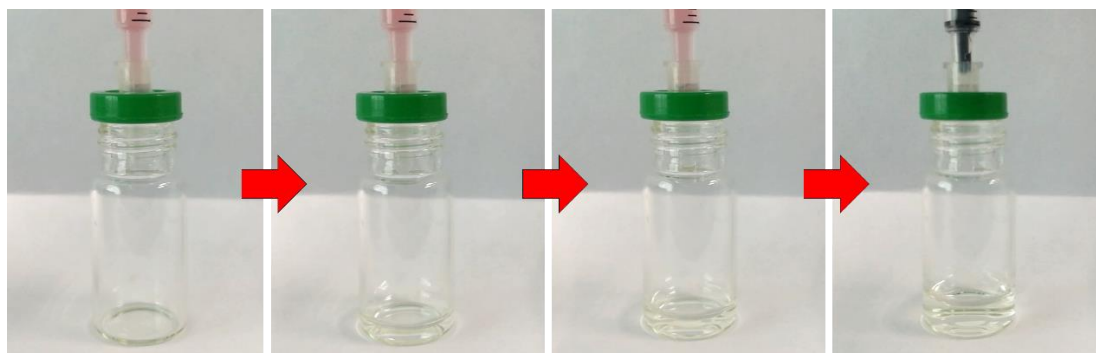
Figure S14. Photographs of the filtration process for 1 mL gold NPs solution (20 nm), related to Figure 5.
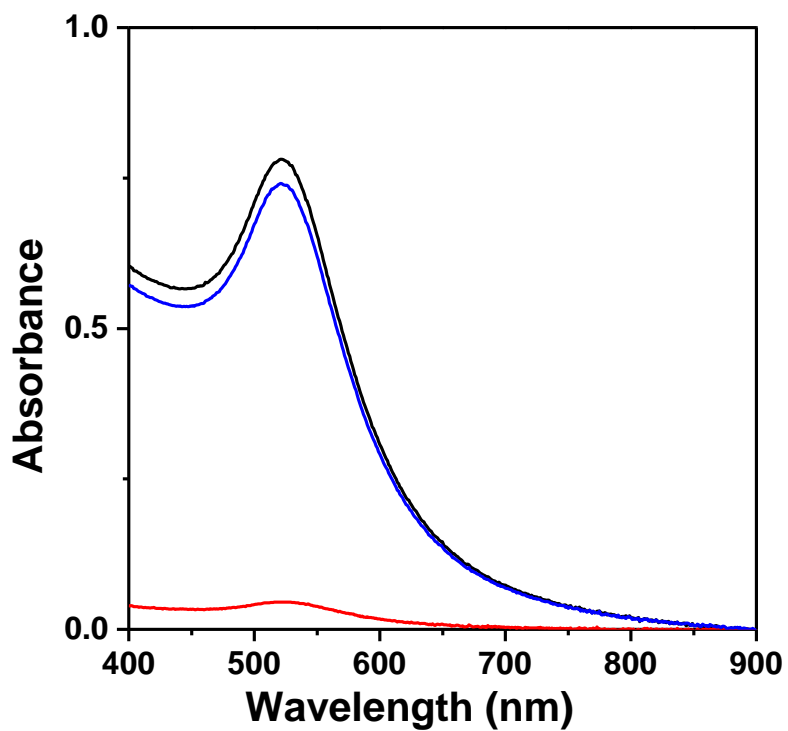
Figure S15. UV-Vis absorption spectra of the 5.5 nm gold NPs solution before (black curve) and the filtrate after filtration by commercial PES film (blue curve) and by PES-supported supramolecular film filter (red curve), related to Figure 5.
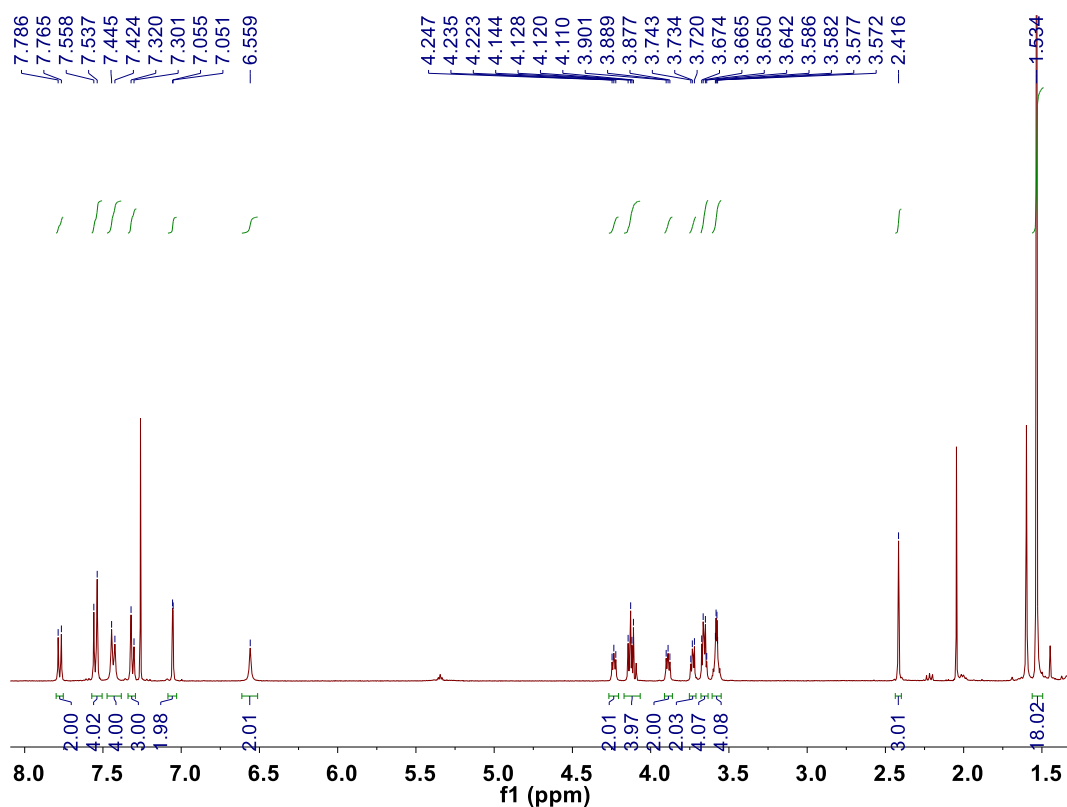
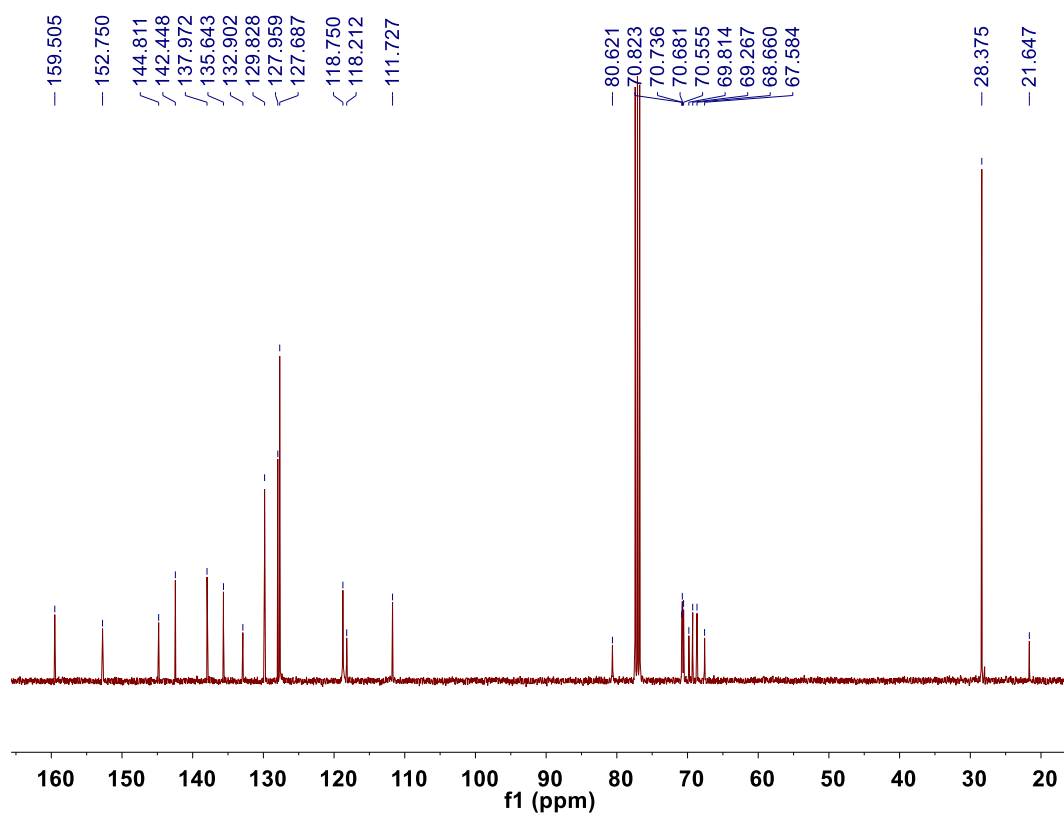**Figure S16.** ^{1}H NMR spectrum of **3** (CDCl$_3$, 400 MHz, 298 K), related to Figure 1.

Figure S17. ^{13}C NMR spectrum of **3** (CDCl$_3$, 100 MHz, 298 K), related to Figure 1.
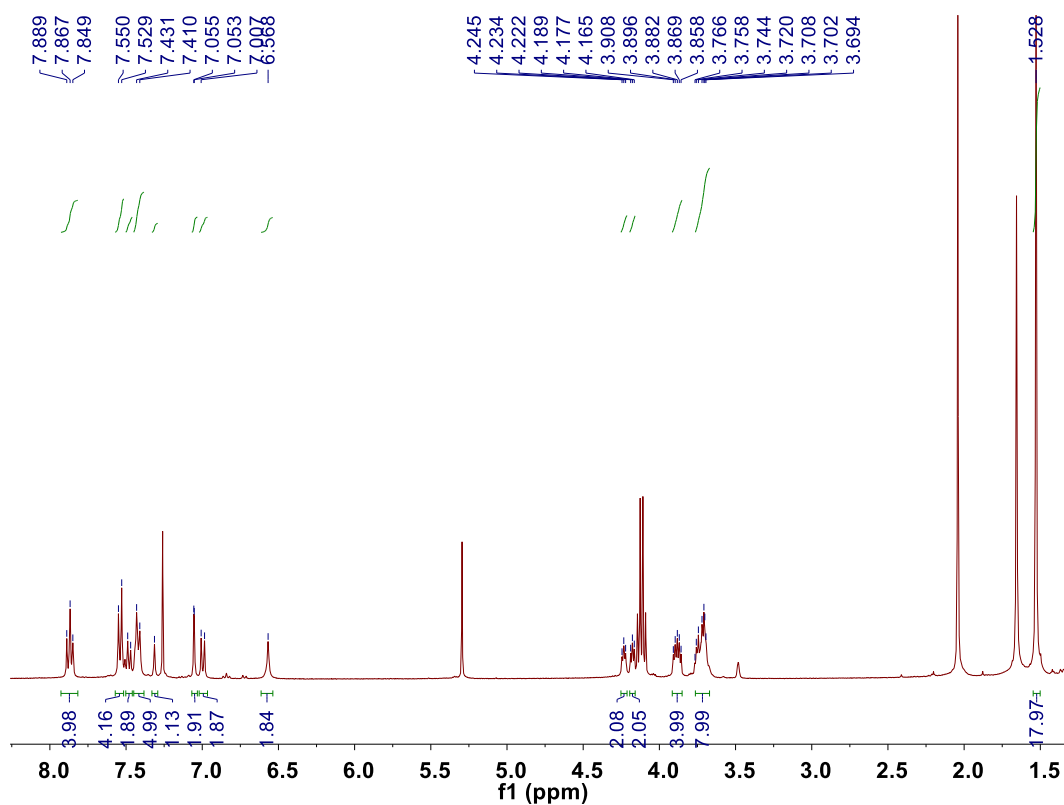
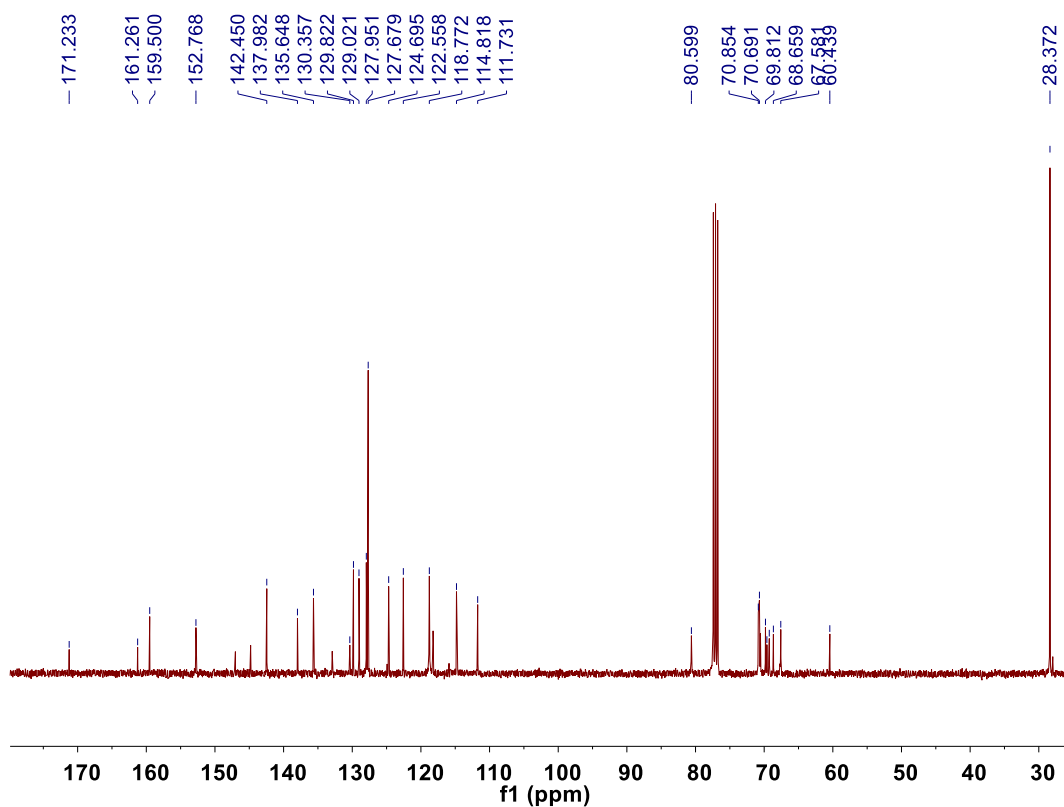**Figure S18.** ^{1}H NMR spectrum of **4** (CDCl$_3$, 400 MHz, 298 K), related to Figure 1.

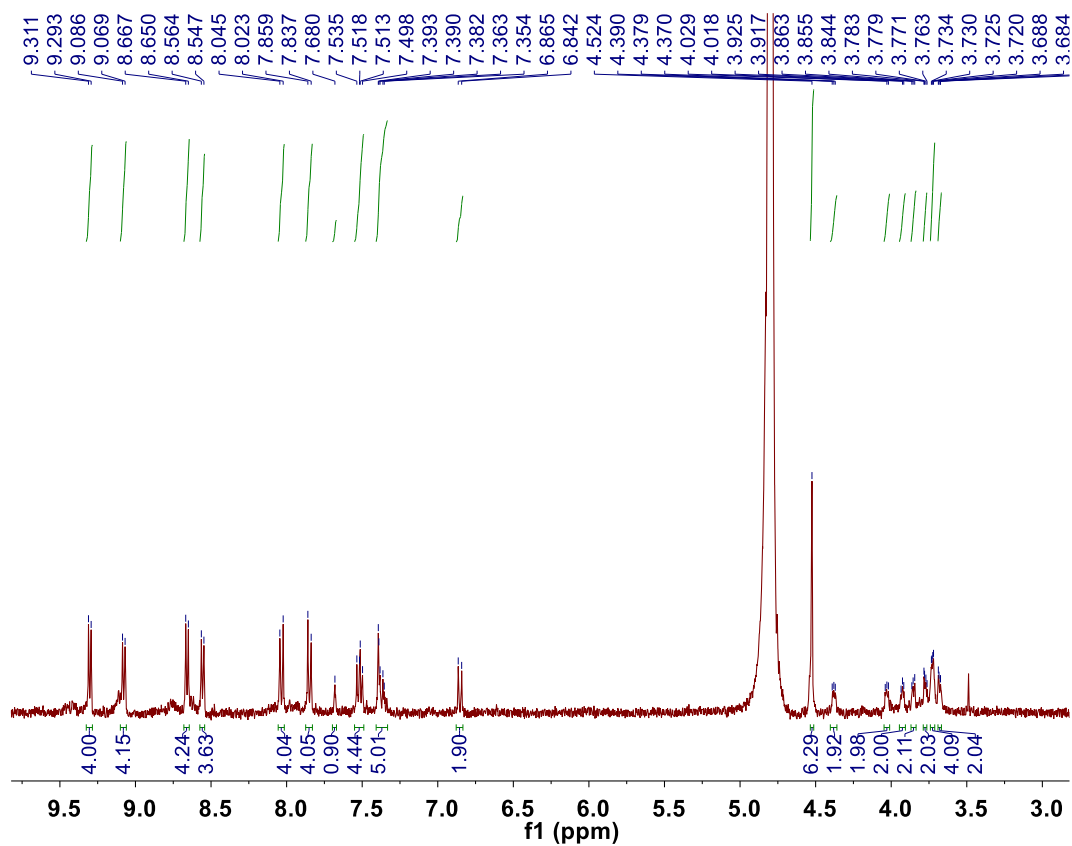**Figure S19.** ^{13}C NMR spectrum of **4** (CDCl$_3$, 100 MHz, 298 K), related to Figure 1.

Figure S20. ^{1}H NMR spectrum of *trans*-**1** (D$_2$O, 400 MHz, 298 K), related to Figure 1.
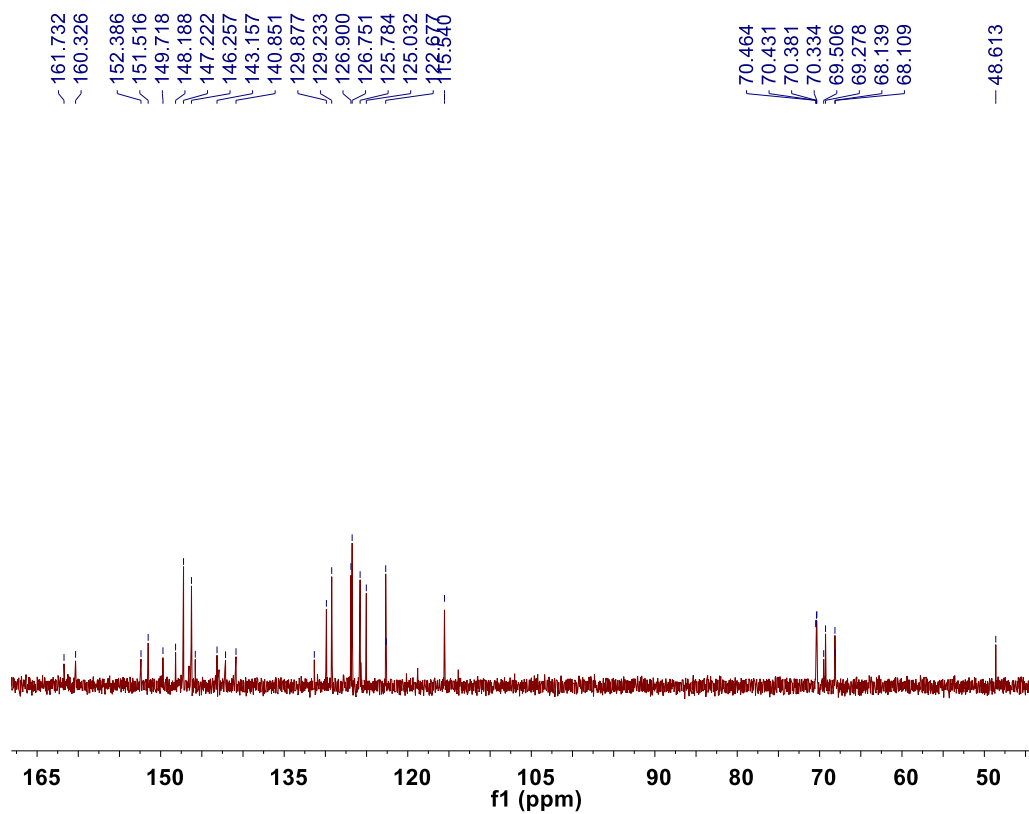

Figure S21. ^{13}C NMR spectrum of *trans*-**1** (D$_2$O, 600 MHz, 298 K), related to Figure 1.